ADVANCED OPTICAL MATERIALS
www.advopticalmat.de

Large Polycyclic Aromatic Hydrocarbons as Graphene Quantum Dots: from Synthesis to Spectroscopy and Photonics

Giuseppe Maria Paternò, Goudappagouda, Qiang Chen, Guglielmo Lanzani, Francesco Scotognella, and Akimitsu Narita**

Synergistic research efforts in multistep chemical synthesis and state-of-the-art optical spectroscopy have permitted the realization of graphene quantum dots (GQDs) with defined structures and properties, paving the way towards their possible applications in photonics and optoelectronics. One such fruitful feedback loop between synthesis and spectroscopy is represented by the recent development of stable GQDs with zigzag edges, displaying excellent spectral features such as optical gain and strong absorption/emission in the visible/near-infrared regions, which are appealing for applications in photonics. In this progress report, the authors provide an overview of the latest developments in the chemical synthesis and advanced spectroscopic investigations of atomically precise GQDs, with particular emphasis on those with zigzag-edged structures. The latest developments in their applications are also introduced, for example, in lasing and optical imaging, and new opportunities in the field of GQDs are discussed, including chiral GQDs with chiroptical properties and possible applications of GQDs for long-lived luminescence. The authors highlight the role and power of chemical synthesis and spectroscopy in providing new GQDs with promising optical properties that pave the way for new and exciting applications in photonics.

1. Introduction

The development of high-performance, stable organic semiconductors (OSCs) for applications in optoelectronics and photonics has been a topic of intense multidisciplinary research in the last three decades, benefitting significantly from progress in organic synthesis, spectroscopy, and materials science.[1–3] The well-known advantages of OSCs over their inorganic counterparts lie essentially in their relatively high absorption coefficient ($\alpha \approx 10^5$ cm^{-1}) and photoluminescence (PL) quantum yield, as well as their high solution processability, which reduces device fabrication costs.[4–6] All these properties could be further tuned and optimized by rational structure design and chemical synthesis, which have permitted extensive utilization of OSCs as active materials in organic solar cells[7–9] and light-emitting diodes (LEDs),[10–12] as well as efficient optical gain media in organic lasers.[13–15]

Large polycyclic aromatic hydrocarbons (PAHs) have emerged in recent decades as unique OSCs with promising optical properties and high chemical and photostability.[16–21] These large PAHs, having discrete quasi-zero-dimensional graphene structures, can also be regarded as graphene quantum dots (GQDs).[22–27] In contrast to zero-bandgap graphene, the quantum confinement of the wave function in GQDs permits the opening of a finite energy gap, conferring appealing features that can be exploited in optoelectronics and photonics, such as a relatively large Frenkel exciton binding energy[28] and multicolor fluorescence.[29–32] In the fields of Materials Sciences, GQDs are

Dr. G. M. Paternò, Prof. G. Lanzani
Center for Nano Science and Technology
Istituto Italiano di Tecnologia (IIT)
Via Pascoli 10, Milano 20133, Italy
E-mail: Giuseppe.paterno@iit.it

The ORCID identification number(s) for the author(s) of this article can be found under https://doi.org/10.1002/adom.202100508.

DOI: 10.1002/adom.202100508

Dr. Goudappagouda, Prof. A. Narita
Organic Optoelectronics Unit
Okinawa Institute of Science and Technology Graduate University
1919-1 Tancha, Onna-son, Okinawa 904-0495, Japan

Dr. Q. Chen, Prof. A. Narita
Max Planck Institute for Polymer Research
Ackermannweg 10, 55128 Mainz, Germany
E-mail: narita@mpip-mainz.mpg.de, akimitsu.narita@oist.jp

Dr. Q. Chen
Department of Chemistry
University of Oxford
Oxford OX1 3TA, UK

Prof. G. Lanzani, Prof. F. Scotognella
Physics Department
Politecnico di Milano
Piazza L. da Vinci 32, Milano 20133, Italy

typically fabricated through solvothermal treatment of small molecular precursors (bottom-up) or "shearing" of graphene sheets (top-down), and their versatile applications have been demonstrated, for example, in the (opto)electronics and biomedicine.[33–37] Nevertheless, GQDs prepared by such methods mostly do not have defined chemical structures, and it is in some cases even difficult to clearly distinguish them from the so-called carbon dots, namely fluorescent carbon nanoparticles.[38,39] GQDs prepared by different methods can have largely different chemical structures, leading to certain controversies in the nomenclature and the discussion of structure-property relationship, particularly the PL mechanism.[34,40,41] In contrast, organic chemistry methods allow the synthesis of large PAHs that can be unambiguously identified, which can also be regarded as monodispersed GQDs with uniform sizes and well-defined chemical structures.[16,25,26,42]

Large PAHs are thus at the interface of OSCs and GQDs, providing a unique opportunity for experimental study of the structure-property relationships of GQDs, which are largely studied by theoretical methods,[43,44] and to explore their applications. The synthesis of large PAHs can be typically carried out through the oxidative cyclodehydrogenation of tailor-made dendritic polyphenylene precursors, which are "planarized" and "graphitized" into disk-shaped molecules consisting of sp^2 carbons.[45] Various PAHs can be obtained by varying the precursor structures and utilizing other synthetic methods, providing structurally defined GQDs with different sizes and edge structures.[16–21] These studies have revealed that not only the size but also the edge structure of GQDs plays a critical role in tuning their optical, electronic, and magnetic properties.[26,46] Specifically, GQDs typically feature two types of edge configurations, namely, armchair and zigzag edges (**Figure 1**). GQDs with only armchair edges mostly have nonmagnetic properties with relatively large energy gaps, while the introduction of zigzag edges can lead to smaller energy gaps with intriguing optical features and even to an open-shell character,[47–50] as demonstrated, for example, by the syntheses of anthenes[51,52] and periacenes.[53–57] Therefore, GQDs with armchair edges hold promise for application in photovoltaics[58,59] and logics, while those with zigzag edges are potential materials for spintronics and photonics.[50,60–63] Although zigzag-edged GQDs typically show low chemical stability,[51,64] the synthesis of an increasing number of examples of stable GQDs with zigzag edges has been demonstrated in recent years, displaying optical properties that are appealing for applications in photonics, such as intense long-wavelength absorption and very bright emission.[49,53,65,66] In this article, we describe the latest developments in the synthesis and spectroscopic characterization of large PAHs as structurally defined GQDs with an emphasis on zigzag-edged structures and optical gain properties. We also introduce new opportunities in chiroptical and long-lived luminescence applications and discuss the potential of GQDs in photonics as promising advanced optical materials.

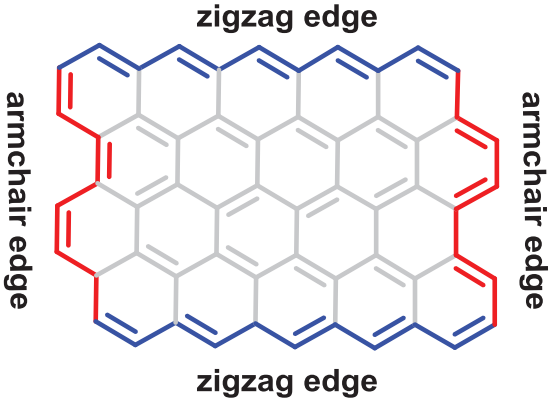

Figure 1. Schematic illustration of armchair and zigzag edges in GQDs.

2. Synthesis, Spectroscopy, and Photonic Applications of Zigzag-Edged GQDs

2.1. Hexa-Peri-Hexabenzocoronene (HBC) Derivatives

Hexa-*peri*-hexabenzocoronene (HBC), as a "superbenzene", has served as the prototypical example of a large PAH and can be considered a representative GQD with only armchair edges.[61] Since almost two decades ago, synthetic approaches have been made to introduce extra K-regions into HBC, namely, additional C2 units, which will form zigzag edges and alter its electronic and optical properties, for example, leading to modulated orbital energy levels and smaller optical gaps.[67–71] While two isomers of HBCs with two K-regions in the "*meta*" and "*para*" configurations and HBC with three K-regions were synthesized, the remaining isomer of HBC with two K-regions in the "*ortho*" configuration and the addition of more than three K-regions remained elusive. In 2016, the synthesis of HBC **6** with four K-regions was achieved with the oxidative cyclodehydrogenation of precursor **5** as the key step, as presented in **Figure 2**.[67] Tetrabromo-*p*-terphenyl **1** was subjected to Suzuki coupling with boronic ester **2** to give triisopropylsilyl-protected precursor **3**. After the deprotection of **3** with tetrabutylammonium fluoride, fourfold Sonogashira-Hagihara coupling with 1-*tert*-butyl-4-iodobenzene yielded precursor **4**. Bis(pyridine)iodonium tetrafluoroborate promoted the fourfold cycloaromatization of **4** to afford diiodinated benzo[*m*]tetraphene dimer **5**. Finally, the oxidative cyclodehydrogenation of **5** using 2,3-dichloro-5,6-dicyano-1,4-benzoquinone (DDQ) as the oxidant together with triflic acid (TfOH) provided HBC **6** with four K-regions.[67] The aromatic core structure of **6** with zigzag edges featured a HOMO-LUMO gap of 2.51 eV, as calculated by density functional theory, which was significantly smaller than the 3.63-eV gap of the parent HBC and demonstrated extended optical absorption up to ≈700 nm, while the latter absorbed only up to ≈400 nm. However, HBC with four K-regions could not be obtained without iodo groups, which quenched fluorescence. Attempts to remove the iodo groups or to use them for coupling reactions also failed, precluding further investigation of the fluorescence properties of HBC with four K-regions.

On the other hand, a stable HBC **10** with two extra K-regions in the "*ortho*" configuration, forming a zigzag edge, could be synthesized, as shown in **Figure 3**.[68] The nucleophilic oxygen/carbon exchange of pyrylium salt **7** led to U-shaped precursor

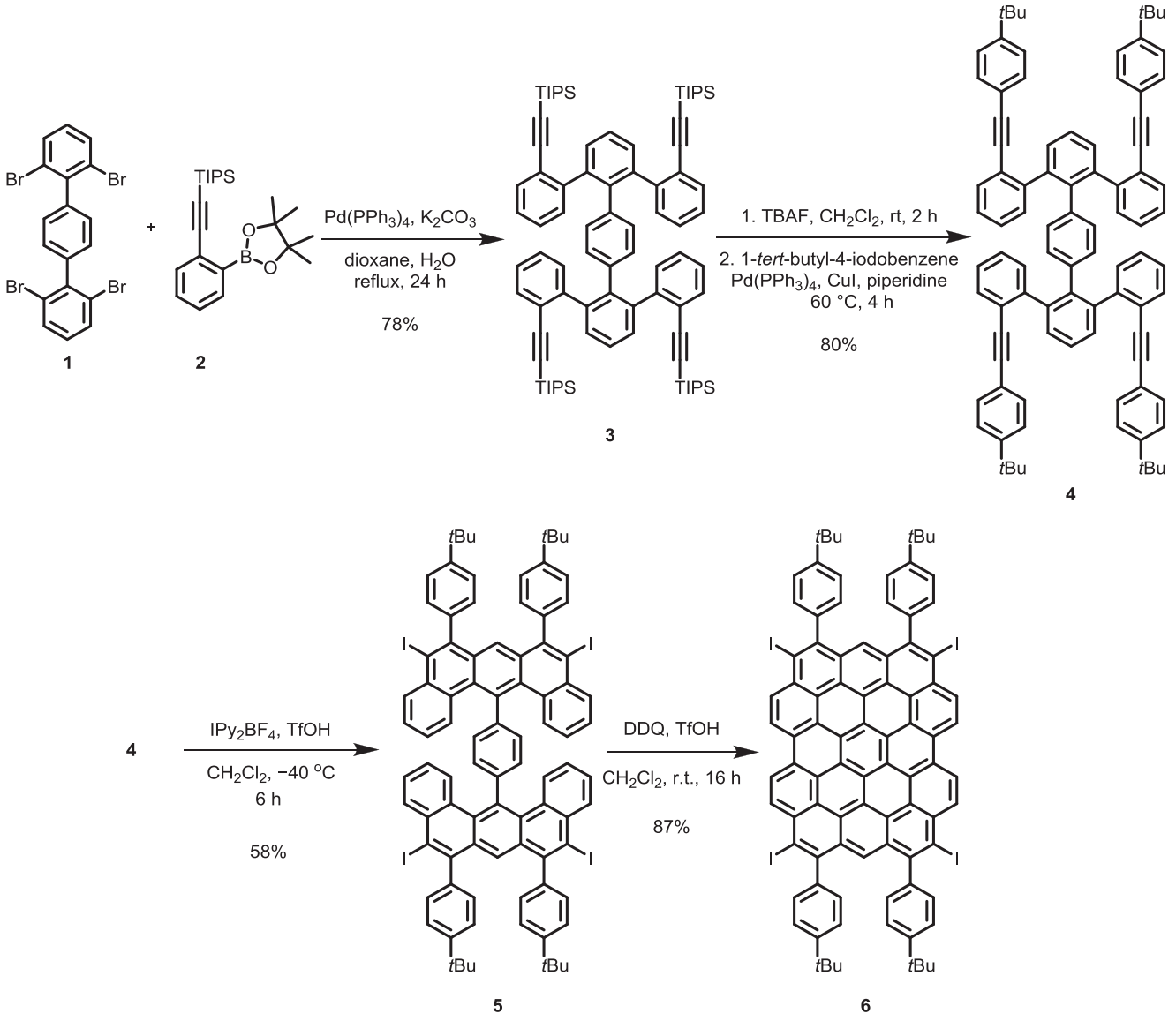

Figure 2. Synthesis of HBC **6** via cyclodehydrogenation of precursor **5** with preinstalled zigzag edges. IPy_2BF_4: bis(pyridine)iodonium tetrafluoroborate.

8 with a zigzag edge. Subsequently, the Suzuki coupling of **8** with 3-*tert*-butylphenylbronic acid provided **9**, which could be "planarized" by oxidative cyclodehydrogenation with DDQ and trifluoromethanesulfonic acid (TfOH) to afford HBC **10**. As expected, the introduction of two K-regions in the "*ortho*"-configuration significantly decreased the HOMO-LUMO gap of **10** to 2.87 eV, which is 0.68 eV smaller than that of the parent HBC. This also agrees with the experimentally observed red-shift of the UV–vis absorption spectrum. Moreover, transient absorption (TA) measurements of **10** permitted us to elucidate the presence of a stimulated emission (SE) signal, which was not obviously observed for the parent HBC.[24] Although the damping of SE was ultrafast (200 fs) and thus would not be useful for actual applications, these findings suggested the importance of zigzag edges to achieve optical gain properties in GQDs (Figure 3b).

2.2. DBOV Derivatives

In 2017, our group demonstrated for the first time the occurrence of optical gain in GQDs. Specifically, we reported dibenzo[*hi*,*st*]ovalene (DBOV) as a new GQD with a combination of armchair and zigzag edges, which revealed strong red emission (637 nm) with a high quantum yield approaching 80%.[72] In the first report, DBOV was synthesized via 12 steps in a linear sequence from commercially available starting materials. Precursor **13b** with two formyl groups was the key intermediate, and its cove edges were converted to zigzag edges through treatment with the mesityl Grignard reagent and subsequent Friedel-Crafts cyclization, followed by oxidation, to yield DBOV **15b** (**Figure 4**). More recently, we have developed an optimized synthetic route to enable gram-scale synthesis of DBOV derivatives (Figure 4).[73] In this new route, the key intermediate

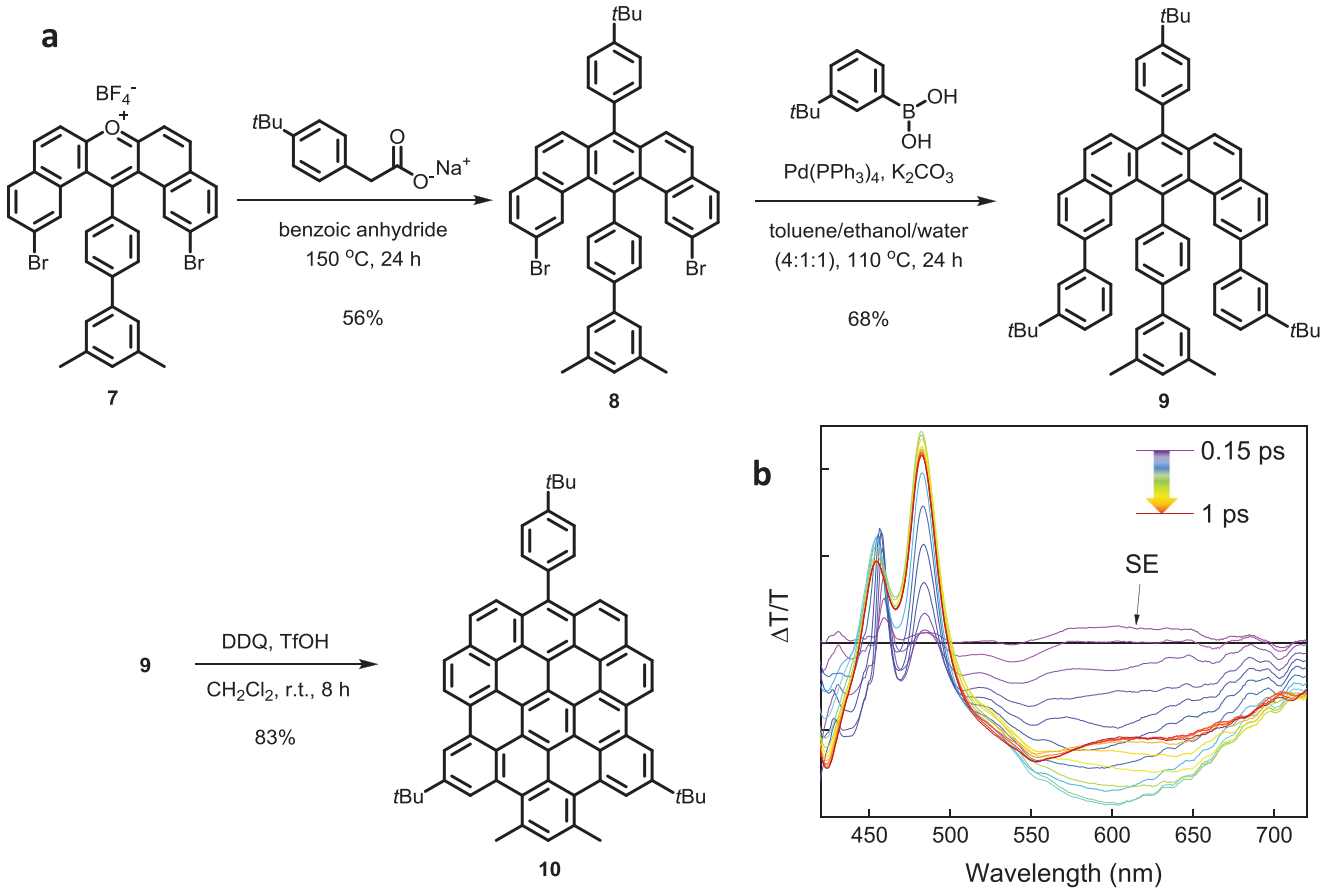

Figure 3. a) Synthetic route for HBC **10**. b) TA measurements highlight the presence of a SE signal for HBC **10**. However, the ultrafast decay (200 fs) hinders its application as an optical gain material. a,b) Adapted under the terms of the Creative Common CC BY license.[68] Copyright 2020, the Royal Society of Chemistry.

13a was synthesized by the iodine monochloride (ICl)-promoted cyclization of diaryldiyne **11** to afford diiodinated bichrysene **12**, followed by photochemical cyclodehydroiodination. This facile and efficient method provided access to various DBOV derivatives with different substituents, including alkyl, aryl, and ethynyl groups, with a total yield of 23–41% over 7 steps.

The TA spectrum of DBOV **15b** measured in a diluted toluene solution revealed an SE signal at 695 nm, while this signal was overwhelmed by a strong absorption from the excited states in a neat film of **15b** (**Figure 5**a).[72] We ascribed these phenomena to ultrafast and nonradiative intermolecular charge-transfer processes in the solid-state that are promoted by strong π–π stacking.[74] To exploit the optical gain properties of DBOV **15b**, we dispersed it in a polystyrene (PS) matrix to minimize intermolecular interactions and aggregation. In a thin film of PS with 1% DBOV **15b**, we could thus observe the recovery of the SE signal and, interestingly, the occurrence of amplified spontaneous emission (ASE) with high operational stability (Figure 5b).[72]

Since the first report in 2017, DBOV derivatives have already been employed in a range of photonic studies, spanning from optical switching[75] to exciton-photon coupling[76] and imaging.[77] For instance, our group has achieved ultrafast all-optical switching with DBOV **15b** by using a three-beam pump-push-pull experiment (**Figure 6**a).[75] Specifically, we exploited the spectral overlap between SE and absorption from dark states with charge separation, which is usually detrimental for the ASE and lasing action in solid-state devices. When the DBOV molecule is adequately isolated, intramolecular geminate recombination of charges allows ultrafast (sub-picosecond) and effective on/off resonant switching. Although the resonant process requires efficient energy dissipation, thus posing critical stability issues, the relatively high photostability displayed by DBOV derivatives can be a key asset for their future applications in plastic optical fibers. The narrow and well-separated optical transitions characteristic of DBOV lend themselves to strong exciton–photon coupling. Indeed, Lidzey and collaborators demonstrated the formation of polariton states upon placing DBOV **15a** into an optical microcavity (at RT), which resulted from the hybridization of the cavity mode with the $0 \rightarrow 0'$ optical transition of **15a** (Figure 6b).[76] These data suggested that the remarkable photostability and high emission efficiency make DBOV an ideal material for generating polariton condensation. Moreover, a recent detailed single-molecule characterization of DBOV permitted access to important details about its photophysics and its potential use as a single quantum emitter.[73] In particular, the fluorescence autocorrelation function displayed high-contrast photon antibunching and bunching (Figure 6c). From these data, the fluorescence decay rate and the triplet population and

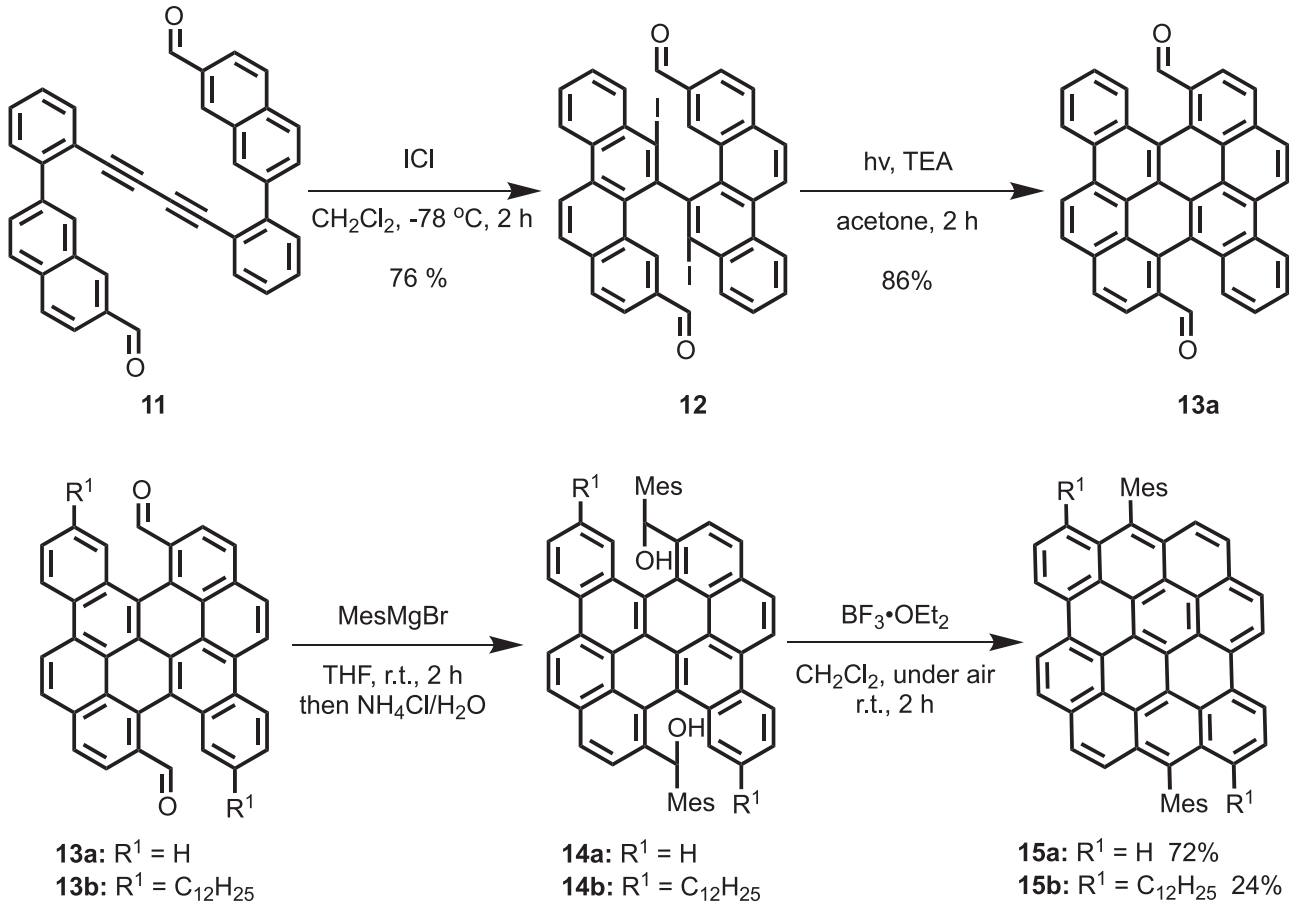

Figure 4. Synthesis of DBOV derivatives **15**. TEA: triethylamine; THF: tetrahydrofuran.

depopulation rates could be retrieved. Interestingly, the intersystem crossing rate into the triplet state decreased by more than an order of magnitude at low temperature, demonstrating that single-photon emission in DBOV can be achieved via temperature control. Applications of DBOV in imaging have also been reported (Figure 6d). The outstanding photophysical properties of DBOV, such as intrinsic blinking even in air, excellent fluorescence recovery, and stability over several months, have rendered it a promising fluorophore for superresolution microscopy.[77] Furthermore, the application of DBOV **15a**, as well as HBC **6**, as a light-absorbing material in all-carbon photodetectors has been demonstrated, where these GQDs were deposited on graphene as the conducting layer (Figure 6e).[78]

Furthermore, postsynthetic functionalization of DBOV **15a** was achieved, starting with its selective bromination at the bay regions.[79] 3,11-Dibromo-DBOV **17** was thus obtained and successfully used for transition-metal-catalyzed coupling reactions to introduce aryl or ethynyl groups (**Figure 7**). Circumarenes are a type of zigzag-edged PAH containing a small aromatic core surrounded by a single layer of benzene rings.[46] Circumarenes with central aromatic core sizes up to three fused benzene rings have been reported, with circumanthracenes as the largest examples to date, reported by Diederich et al. in 1991[57] and then Feng et al. in 2018.[53] In 2020, our group reported the successful synthesis of a new member of the circumarene family, namely, a circumpyrene, by the π-extension of DBOV.[80] Circumpyrene **20** could be obtained through the twofold palladium (Pd)-catalyzed benzannulation of 3,11-dibromo-DBOV **17** with diphenylacetylene, together with monoadduct **19** (Figure 7). The π-extension from DBOV to **19** and then **20** increased the optical and electrochemical energy gaps, accompanied by blueshifts in the optical absorption and emission (Figure 7). These results highlighted the significance of the postsynthetic π-extension of GQDs to selectively obtain novel GQD structures, thereby modulating the optoelectronic properties. The possible optical gain properties and other photophysical characteristics of **19** and **20**, as well as aryl-substituted DBOV 18 with different functional groups, are currently under investigation in our laboratories.

2.3. GQDs with Four Zigzag Edges (FZ)

Recently, Wu and his colleagues demonstrated a systematic synthesis of a series of GQDs having four zigzag edges (FZs), including **FZ1**, **FZ2**, and **FZ3** (**Figure 8**).[65,66] For the synthesis of **FZ1**, dialdehyde **24** was prepared from diol **23** through Swern oxidation. Dialdehyde **24** was then treated with mesitylmagnesium bromide and quenched with water to give a diol intermediate, followed by intramolecular Friedel–Crafts

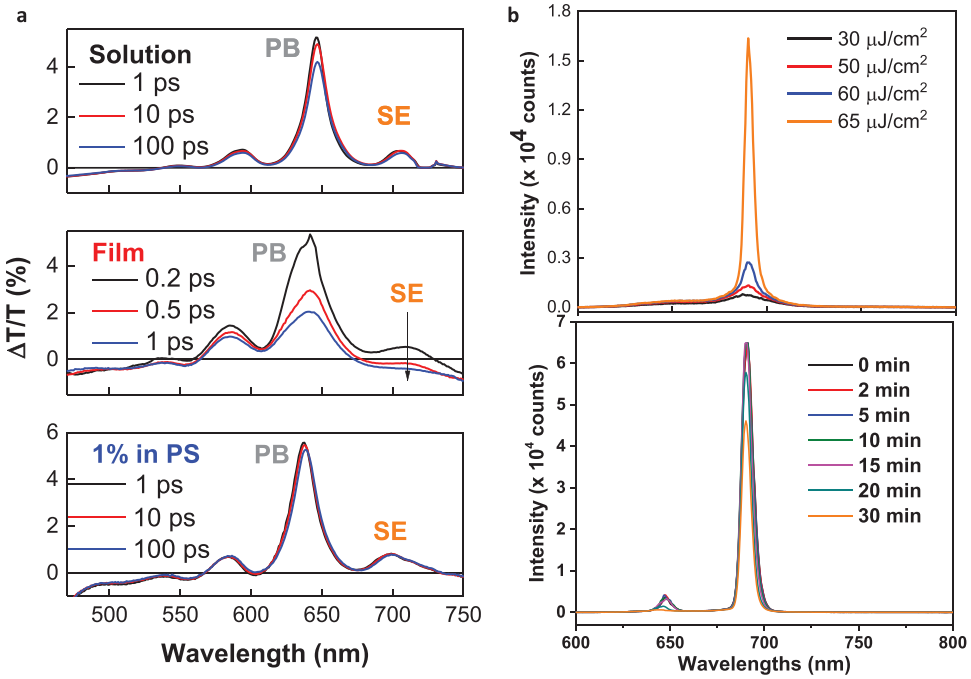

Figure 5. a) TA spectra of DBOV in diluted toluene solution, in a solid neat film, and in a blend with PS. Although the SE signal is overwhelmed by excited-state absorption in the neat film, this feature can be recovered by suppressing the intermolecular interactions in the PS matrix (1% blend). b) ASE action in the DBOV **15b**:PS blend. Notably, ASE with high operational stability is observed (only 30% decay after 30 min of intense irradiation (2×10^6 pulses, at 320 μJ cm^{-2})). Reproduced with permission.[72] Copyright 2017, Wiley-VCH.

cyclization to provide intermediate **25**. In the final step, **FZ1** was obtained by the dehydrogenation of **25** with *p*-chloranil as the oxidant (Figure 8a). **FZ2** and **FZ3** were also synthesized in a similar manner, through tetraaldehydes **27** and **30**, respectively (Figure 8b,c). The zigzag edges of **FZ1**, **FZ2**, and **FZ3** are kinetically protected by bulky aryl groups, and these functional groups ensure their adequate stability and solubility.[66]

FZ1, **FZ2**, and **FZ3** have shown intriguing photophysical properties that can be appealing for photonic applications, similar to the case of DBOV derivatives. Moreover, analysis of their ASE spectra revealed a change in the emission mechanism as a function of the molecular size, with the larger **FZ3** displaying ASE from the first vibronic replica (0′ → 0 transition) and not from the second (0′ → 1 transition), as in the cases of **FZ1** and **FZ2** as well as most other organic dyes (**Figure 9**b).[72] The authors attributed this phenomenon to changes in the electron-vibration mechanism along the relevant electronic excitation, related to the more extended 2D π-electron delocalization in **FZ3** than in **FZ1** and **FZ2**.[62] Furthermore, these **FZ**-GQDs were blended in a PS matrix to attain lasing action. Specifically, the authors employed a fully solution-processed distributed feedback laser (DFB) based on a top-layer resonator (Figure 9c). Notably, efficient lasing was observed from the blue to the near-infrared (NIR) region. These GQDs also showed excellent environmental stability (i.e., against air and moisture) and photostability, exhibiting an outstanding operational lifetime. Very recently, **FZ3** was demonstrated to sustain dual ASE and lasing at both 685 and 749 nm, even though the excitation threshold to achieve ASE was 10 times larger than those observed for **FZ2** and **FZ3**.[81] This high threshold could be attributed to the spectral overlap between gain and absorption from charge-separated states in the NIR.

2.4. Perylene-Fused GQDs with Partial Zigzag Peripheries

In 2020, the groups of Díaz-García and Wu showed that lasing action in the visible could be attained by using aggregation-free perylene-fused GQDs **ZY-01** and **ZY-02** with partial zigzag peripheries (**Figure 10**).[82] The introduction of a C(sp^3)-bridged five-membered ring at the bay region of the perylene moiety, as reported previously by Wu and his colleagues,[83] suppressed the aggregation of these GQDs, thus minimizing the aggregation-induced PL quenching. GQDs **ZY-01**, **ZY-02**, and **ZY-03** were synthesized as shown in Figure 10a. Ethynyl-substituted perylene derivative **32** was initially prepared as the key intermediate, and subjected to the Diels–Alder cycloaddition with tetraphenylcyclopentadienone **33** to provide precursors **34** in 78% yield. Interestingly, oxidative cyclodehydrogenation of **34** by using DDQ and methanesulfonic acid ($MeSO_3H$) in dichloromethane (CH_2Cl_2) at room temperature (RT) selectively resulted in the partially fused product **ZY-01** in 85% yield. Prolonging the reaction time did not yield the fully fused product **ZY-02**, but the use of iron(III)chloride in nitromethane/CH_2Cl_2 gave **ZY-02** in 36% yield from precursor **34**. In addition, **ZY-02** could also be obtained through treatment of **ZY-01** with iron(III)chloride in 50% yield. **ZY-03** was synthesized through the Diels–Alder reaction of **32** with biscyclopentadienone **35** to afford precursor **36** in 38% yield, followed by the oxidative cyclodehydrogenation with DDQ and $MeSO_3H$ in CH_2Cl_2 at RT to give **ZY-03** in 78% yield. Similar to the above-described case of FZs, the authors exploited a solution-processed DFB device to achieve lasing action in the visible (515–523 nm) from **ZY-01** and **ZY-02**, which displayed the optical gain (Figure 10b) while **ZY-03** did not show net gain due to the overlap between

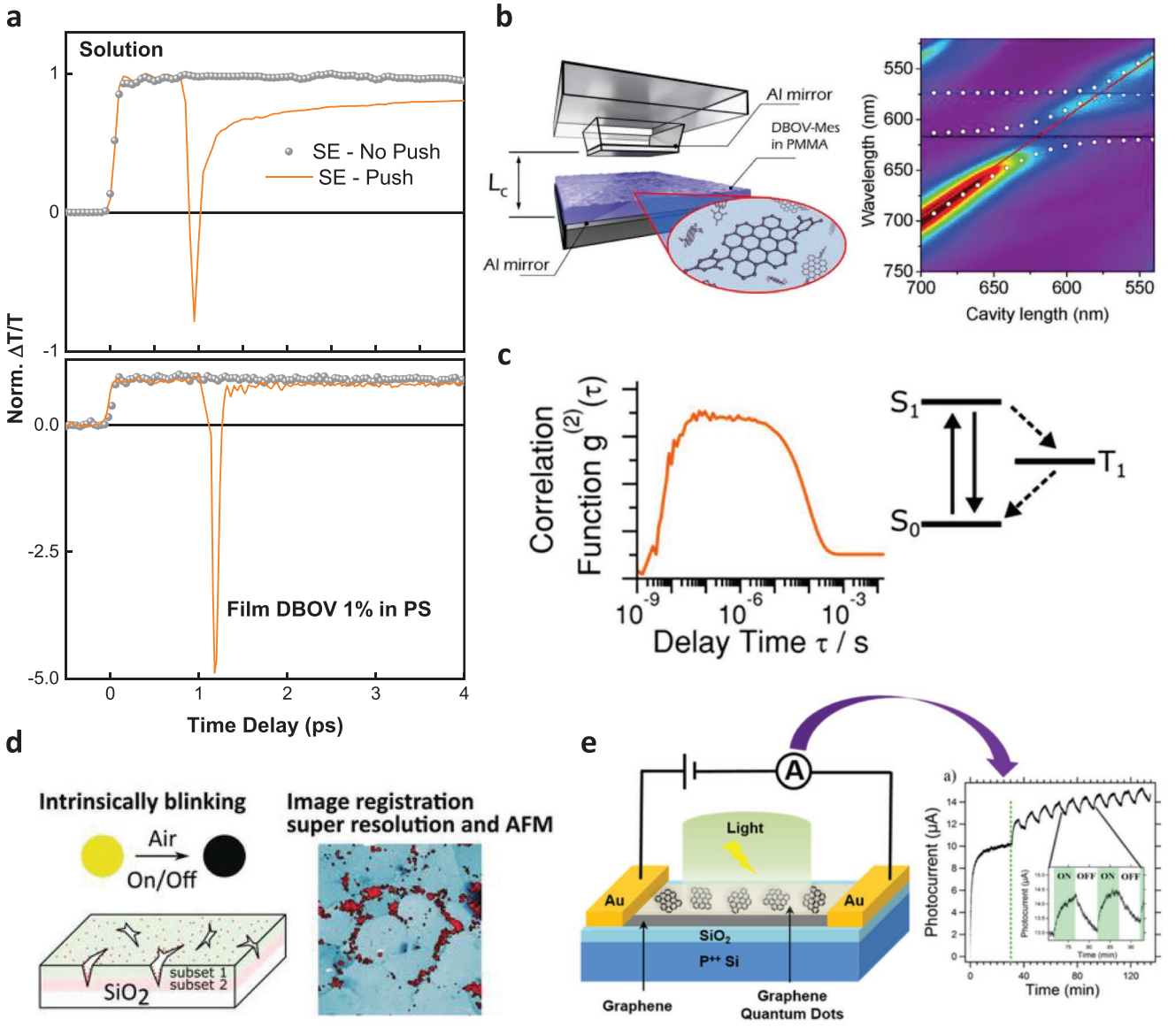

Figure 6. a) All-optical switching in DBOV **15b** solution and DBOV:PS film by using the three-beam pump-push-probe technique. Adapted with permission.[75] Copyright 2019, Wiley-VCH. b) Exciton–photon coupling is achieved by filling an optical microcavity with DBOV **15a**. c) Single-molecule spectroscopy on a DBOV derivative with 2,6-dimethylphenyl groups reveals the potential of this molecule as a single quantum emitter. Reproduced under the terms of the Creative Common CC BY license.[73] Copyright 2019, American Chemical Society. d) Application of DBOV **15a** in superresolution microscopy. Reproduced under the terms of the Creative Common CC BY license.[77] Copyright 2019, The Authors, published by Wiley VCH. e) Color-sensitive photodetector fabricated by using DBOV **15a** as a light-absorbing material. Reproduced with permission.[78] Copyright 2019, American Chemical Society.

SE and absorption from excited states that were attributed to triplets.

3. New Opportunities for GQDs in Photonics

3.1. π-Truncation of GQDs

Novel synthetic approaches towards the development of advanced functional GQDs are currently being deployed. For instance, we have recently reported the synthesis of peralkylated GQD **38** via the regioselective hydrogenation of GQD **37** with 60 contiguous sp^2 carbons in its aromatic core (**Figure 11**a).[84] The hydrogenation of **37** was carried out with Pd/C in dry tetrahydrofuran (THF) at 120 °C, which could be completed either in two weeks at 120 bar and 120 °C or in one week at 150 bar (Figure 11a). While most of the GQDs were synthesized through the "π-expansion" of smaller aromatic molecules, this synthesis of GQD **38** with 38 sp^2 carbons from GQD **37** with the larger aromatic core can be considered a rare example of "π-truncation", which can potentially extend the scope of GQD synthesis. In addition to the novelty of the synthetic method, we showed that peralkylated GQD **38** holds potential for future applications in photonics. Specifically, TA measurements indicated that GQD **38** displays an SE signal at 500 nm, whereas absorption from excited states overwhelms the SE in the case of

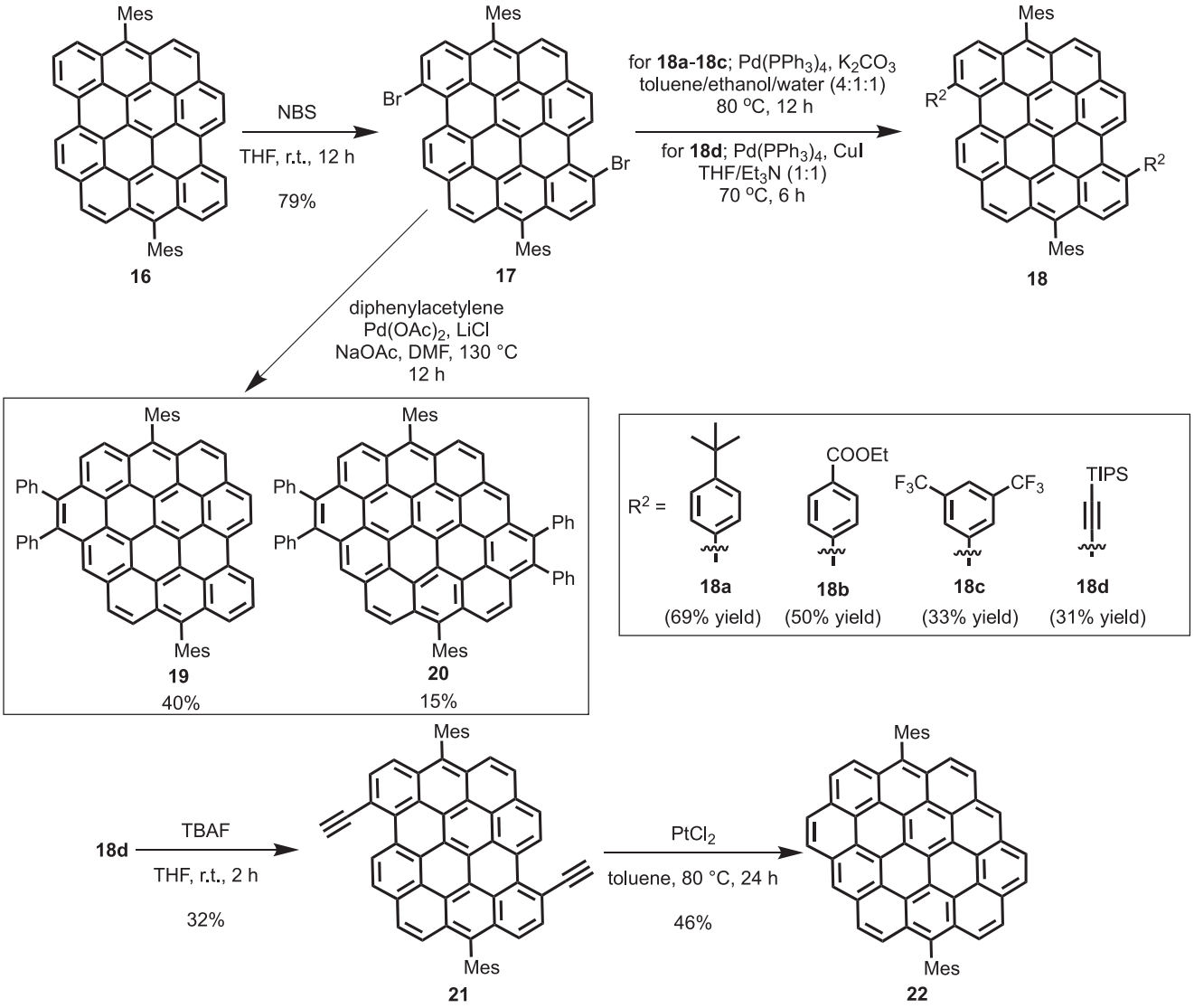

Figure 7. Selective bromination of DBOV-Mes **16** at the bay positions, post-functionalization of DBOV by cross-coupling reactions, and synthesis of circumpyrenes **20** and **22**. DMF: dimethylformamide; THF: tetrahydrofuran.

GQD **37** (Figure 11c). The reason GQD **38** displays SE likely lies in its improved solubility brought about by the peripheral alkyl groups as well as the smaller aromatic core, based on our previous observation in DBOV derivatives with different solubilities that intermolecular interactions can lead to the formation of aggregates with charge-transfer character, where the charge generation quenches the SE and gain.[74]

3.2. π-Extended Helicenes as Chiral GQDs

Nonplanar GQDs represent another important class of molecules that display unique features, such as optoelectronic properties, conformational dynamics, and intriguing supramolecular characteristics, which are distinct from those of planar GQDs.[56] Chirality can also arise in nonplanar π-conjugated structures with chiral axes, which is among the most appealing features of such systems. For example, field-effect transistors based on chiral π-conjugated molecules can be utilized to detect circularly polarized light, which is intrinsically difficult with conventional photodetectors.[85] In this case, the nonplanar core has to ensure both efficient π-stacking, to guarantee efficient intermolecular charge/electron transfer, and extended π-conjugation. Moreover, chiral GQDs could also find potential application for in vivo bioimaging and NIR light-emitting devices, where NIR-emitting systems could be especially interesting.

Helicenes, consisting of consecutive *ortho*-condensed aromatic rings, are among the most studied nonplanar chiral π-conjugated molecules.[86] Helicene derivatives with extended aromatic structures have recently attracted growing attention, including both π-extended single helicenes and molecules containing multiple helicene moieties, which display enhanced chiroptical responses and/or unique self-assembling characteristics distinct from those of single helicenes.[87–96] Nevertheless, there are still only a few examples of reported multihelicenes

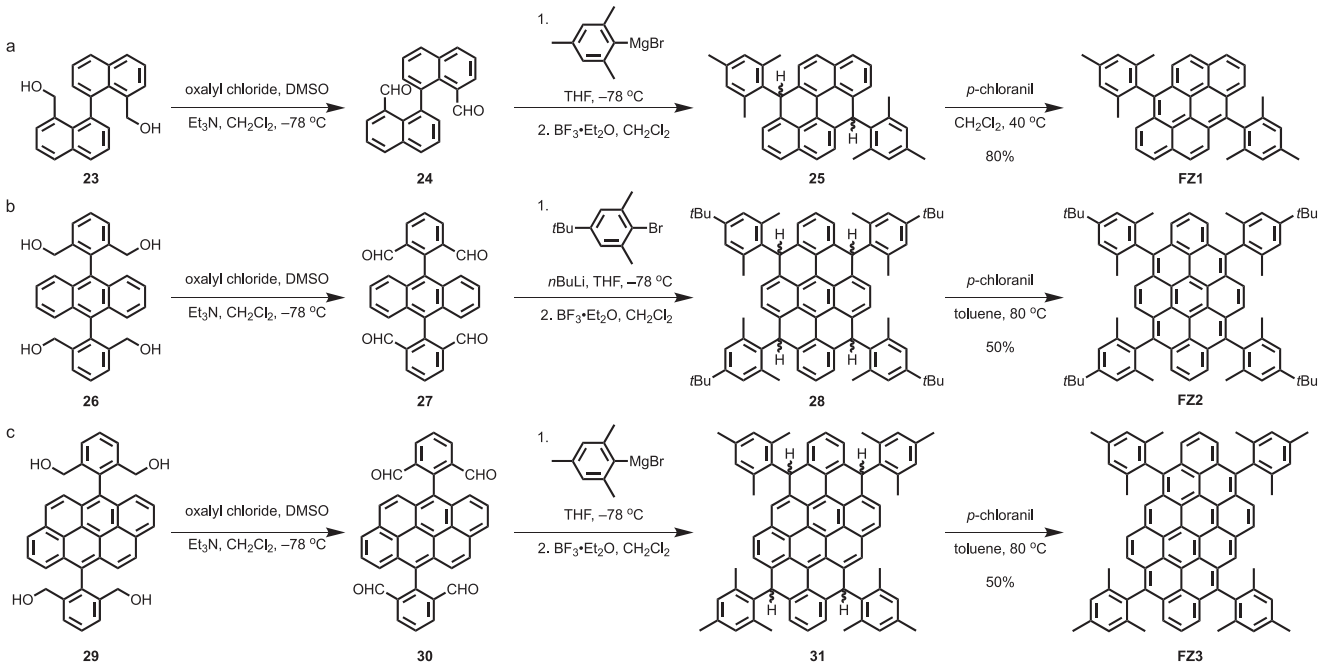

Figure 8. Synthetic routes towards a) **FZ1**, b) **FZ2**, and c) **FZ3**. DMSO: dimethylsulfoxide; THF: tetrahydrofuran.

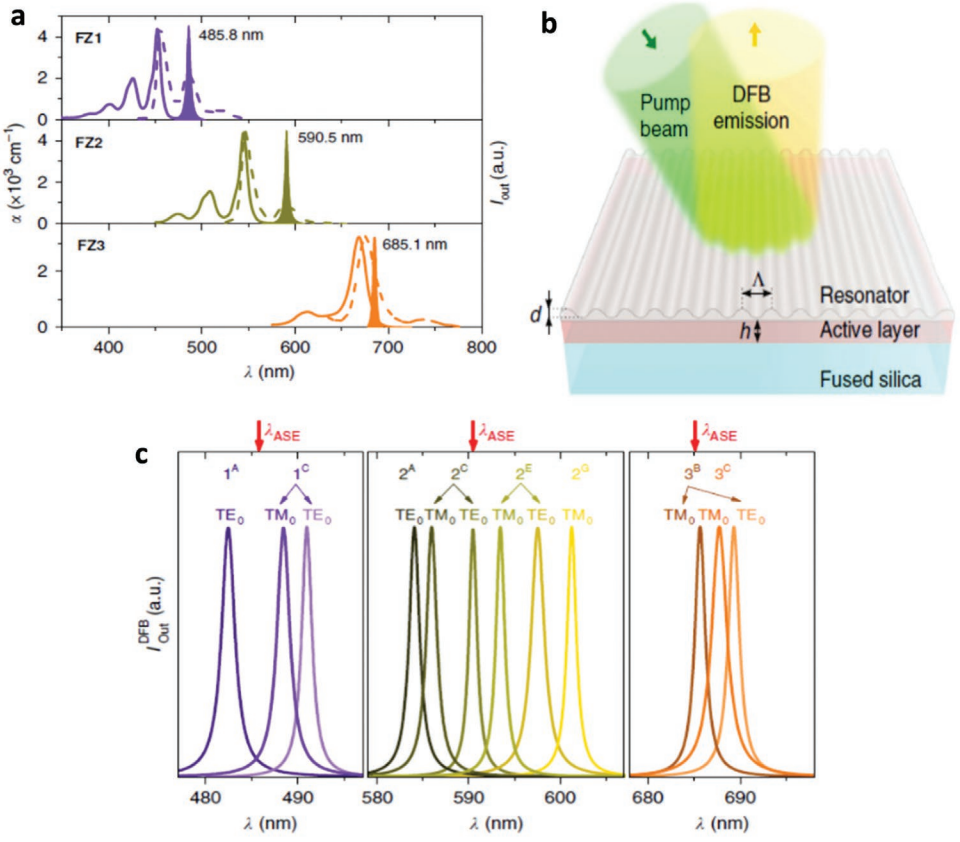

Figure 9. a) Molecular structures of **FZ1**, **FZ2**, and **FZ3**. a) Absorption, PL, and ASE spectra of the three **FZ**-GQDs. b) Sketch of the DFB resonator, consisting of a top-layer polymeric resonator with an engraved relief grating (Λ, grating period; d, grating depth), located over an active film (h, film thickness) of GQDs dispersed in PS, deposited on a fused silica substrate. c) Spectra of the DFB lasers based on **FZ1**, **FZ2**, and **FZ3** (indicated as 1, 2, and 3 in the Figure). The laser line consists of either one or two peaks (modes), each associated with a given waveguide mode of the film, TE_0 or TM_0, whose light is polarized parallel or perpendicular to the DFB grating lines, respectively. The top red arrows indicate the ASE wavelength for each case. Reproduced with permission.[62] Copyright 2019, Springer Nature.

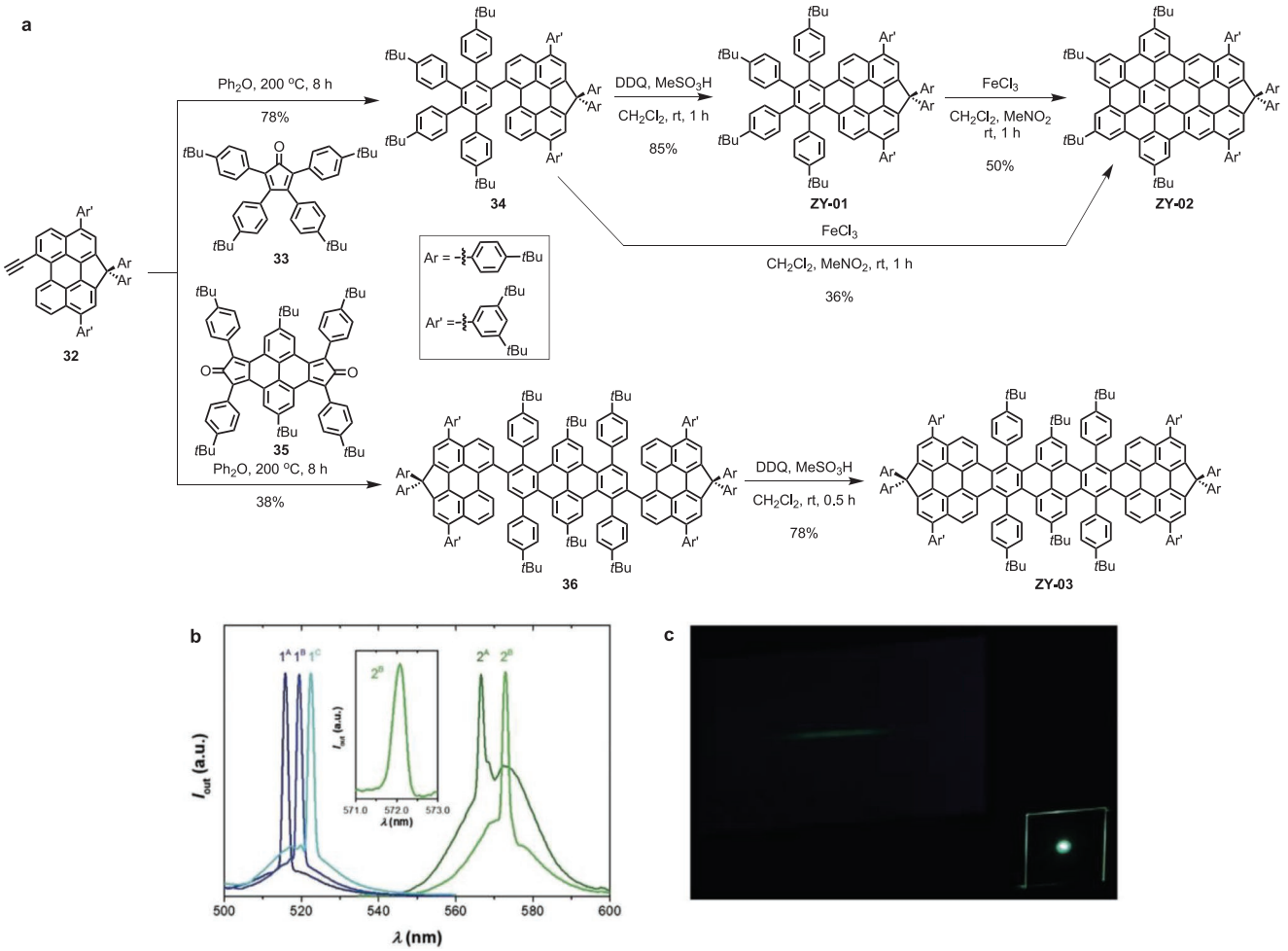

Figure 10. a) Synthetic routes towards **ZY-01**, **ZY-02**, and **ZY-03**. b) Spectra of the DFB lasers in which the active material is **ZY-01** (blue lines) and **ZY-02** (green lines). The number on the device label (1 or 2) refers to the compound used (**ZY-01** or **ZY-02**, respectively), while the letters on the labels refer to devices with different geometrical parameters, as reported in Ref. [82]. c) Picture of the green light emitted by laser 1^A, projected on a screen in the left top corner. The bright spot in the center of the sample is a mixture of the pump and emitted laser light. Reproduced with permission.[82] Copyright 2020, Wiley-VCH.

with efficient intra- and intermolecular π–π interactions and/or NIR emission.[97,98] In 2017, the synthesis of double [7]carbohelicene **41** was achieved in two steps, starting from tetrabromoterphenyl **39** (**Figure 12**a).[99] First, **39** was subjected to a fourfold Suzuki coupling reaction with 2-naphthylboronic acid pinacol ester to provide tetranaphthyl-*p*-terphenyl **40** in 85% yield. Then, the intramolecular oxidative cyclodehydrogenation of precursor **40** using DDQ and TfOH regioselectively yielded double [7]carbohelicene **41** (Figure 12a).

More recently, we reported the synthesis and characterization of a π-extended double helicene **43** with fused pyrene substructures in a similar manner to the preparation of **41**, employing 2-pyrenylbornic acid pinacol ester as the coupling partner of **39** (Figure 12a).[100] π-Extended double helicene **43** featured a broad and highly redshifted emission in the NIR (from 600 to 900 nm) compared to that of **41** at 565 nm. This unique fluorescence of **43** was tentatively ascribed to the formation of an intramolecular excimer based on TA spectroscopy analyses. In addition, this system displayed a relatively high chiroptical stability, as indicated by the high isomerization barrier of 46.3 kcal mol^{-1} (Figure 12c). This allowed separation of the enantiomers with opposite helicity, as confirmed by mirror-symmetric circular dichroism spectra. The chiroptical properties and the enhanced intra- and intermolecular π–π interactions can enable the application of [7]carbohelicene as a chiral semiconducting and light-emitting material.

3.3. GQDs for Long-Lived Luminescence

One of the research areas in which OSCs excel is room-temperature phosphorescence (RTP).[101–104] Such systems hold great potential for applications in organic photonics, with possible use, for example, in bioimaging, lighting, nonlinear optics, and lasing.[105,106] The recent past witnessed a very large jump in the new molecular design and exploration of organic phosphors,[105,107–112] demonstrating RTP that persists longer than 100 ms with an afterglow and even exceeds the lifetime of 1 s after cessation of excitation.[58,60,113] This ultralong RTP property is enabled by the specific molecular organization of

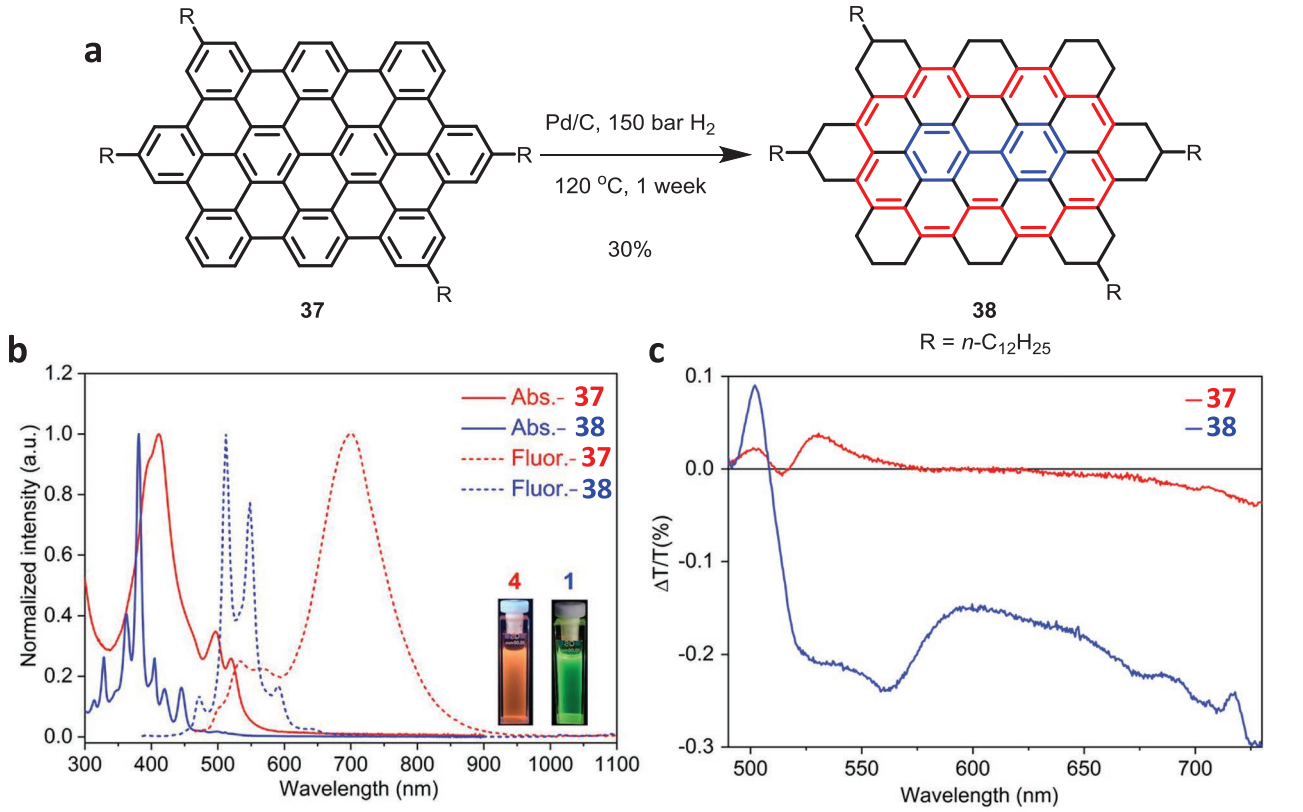

Figure 11. a) π-Truncation of GQD **37** to peralkylated GQD **38**. b) UV–Vis absorption and PL of GQDs **37** and **38**. c) TA spectra (taken at 1 ps) of GQDs **37** and **38** displaying the presence of SE for GQD **38**. a–c) Reproduced under the terms of the Creative Common CC BY license.[84] Copyright 2019, American Chemical Society.

OSCs using a proper host material, which stabilizes the excited triplet state, prolonging both their radiative and nonradiative lifetimes.[114–116] The RTP of PAHs has been studied over decades,[117–119] but the application of coronene (**44**, **Figure 13**a) has recently been revisited to achieve long-lived RTP using new host materials,[120,121] indicating the potential of such PAHs in this field of photonics. On the other hand, the RTP features of conventional GQDs and carbon dots have also attracted attention, as summarized by a recent review article by Yang, He, Ding, and their colleagues, including the discussion of the mechanism and potential applications.[34]

In 2016, the Adachi group reported 3-(*N*-carbazolyl)-androst-2-ene (CzSte) as a new host material while using coronene-d_{12} (**45**) as the RTP emitter, demonstrating an extended phosphorescence lifetime (τ_p) of 4.7 s and a phosphorescence quantum yield (ϕ_p) of 5.3% (Figure 13a,b).[120] The planar structure of **45** was found to be suitable for efficient intermolecular CH-π interactions with the steroid moiety of the CzSte-based host, which presumably suppressed the molecular vibration and thus the nonradiative decay of **45**. Furthermore, LED devices could be fabricated using the prepared host-guest **45**@CzSte samples, displaying electroluminescence from **45** during electrical excitation, followed by RTP with an afterglow lifetime of 4.3 s after turning off the voltage (Figure 13c). On the other hand, Hirata and Vacha reported a τ_p of 17 s for coronene-d_{12} (**45**) embedded in β-estradiol as the host as well as efficient accumulation of triplet excitons, which led to reverse saturable absorption, causing a decrease in the optical transmittance even by weak excitation with similar power to that of sunlight.[122,123]

Metal–organic frameworks (MOFs) are promising porous materials that can serve as hosts of various guest molecules for multiple applications.[124–126] Kabe, Adachi, and coworkers proposed the use of an MOF, in particular a zeolitic imidazolate framework (ZIF-8), as a host for RTP emitters and demonstrated a long-lived RTP from coronene (**44**) with a τ_p of 7.4 s.[121] Moreover, an extended lifetime of 22.4 s was achieved for coronene-d_{12} (**45**) in ZIF-8 under the same experimental conditions. The enhanced lifetime of **45**@ZIF-8 was ascribed to the lower vibrational energy of the C-D stretching mode compared to the C-H stretching mode.[127] Additionally, temperature-dependent lifetime measurements confirmed the suppression of nonradiative deactivation of coronene (**44**) by encapsulation in ZIF-8.

Moreover, in 2020, Kuila and George proposed another approach to achieve long-lived luminescence through triplet-to-singlet Förster resonance energy transfer (FRET), where coronene tetracarboxylate salt (CS) **48** was employed as the triplet energy donor.[128] For the synthesis of CS **48**, perylene (**46**) was subjected to twofold Diels–Alder cycloaddition with *N*-ethylmaleimide followed by oxidation, to give coronene diimide **47**, which was further treated with KOH in methanol to yield **48** (**Figure 14**a). After embedding in a poly(vinyl alcohol) (PVA) matrix, CS **48** showed RTP in the range of 500–700 nm with

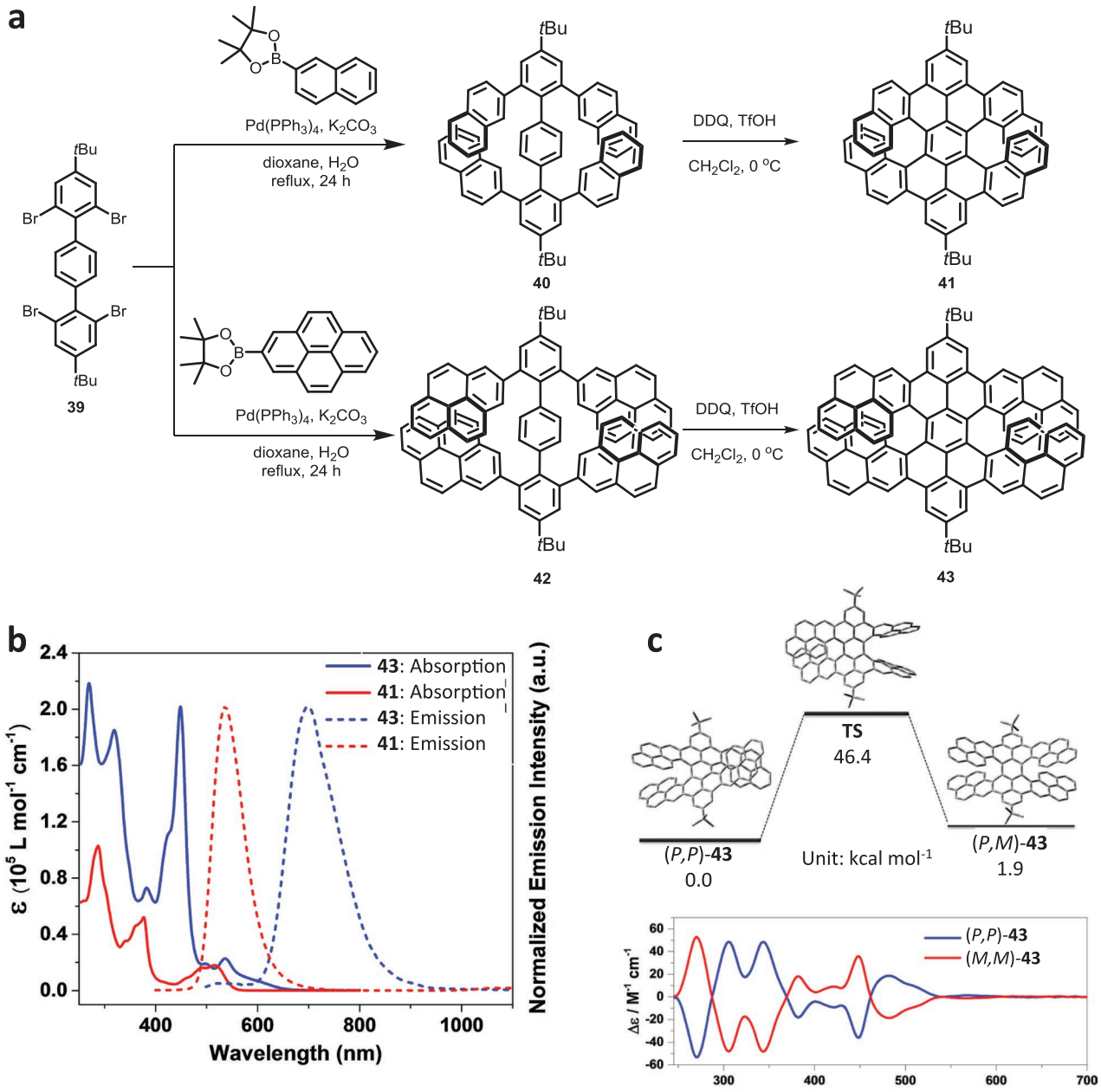

Figure 12. a) Synthesis of double [7]carbohelicene **41** and π-extended double [7]carbohelicene **43** through the cyclodehydrogenation of **40** and **42**, respectively. b) UV–Vis and PL spectra of **41** (red) and **43** (blue). c) Isomerization process between (*P*,*P*)-**43** and (*P*,*M*)-**43** with calculated relative Gibbs free energy. d) Experimental circular dichroism spectra of (*P*,*P*)-**43** and (*M*,*M*)-**43**. b,d) Reproduced under the terms of the Creative Common CC BY license.[100] Copyright 2019, American Chemical Society.

an average τ_p of 2.46 s and ϕ_p of 23.4% (Figure 14b). The commercial rhodamine dyes sulfarhodamine G (SRG, **49**) and sulfarhodamine 101 (SR101, **50**), were selected as acceptors for the phosphorescent energy transfer from CS **48** because of the favorable overlaps of their optical absorption and the RTP bands of **48** as the donor. When 1.0 to 10.0 wt.% SR101 **50** with respect to CS **48** was used in the PVA matrix, the emission spectra of the CS **48**/SR101 **50**/PVA films displayed an attenuation of the phosphorescence bands of **48** together with an enhancement of the emission from SR101 **50** at 550–700 nm (Figure 14c), indicating FRET from the triplet state of **48** to the singlet state of SR101 **50**. The occurrence of nonradiative FRET was further corroborated by the decrease in the average lifetime from 2.46 to 1.33 s and then to 0.86 s as the ratio of SR101 **50** was increased from 0 to 5.5 wt.% and then to 10.0 wt.%, which excluded the possibility of the emission-reabsorption process. The thin films of CS **48**/PVA, CS **48**/SRG **49**/PVA, and CS **48**/SR101 **50**/PVA were self-supporting and flexible, demonstrating stable afterglow features in greenish-yellow, yellow, and red, respectively (Figure 14b). The same group also

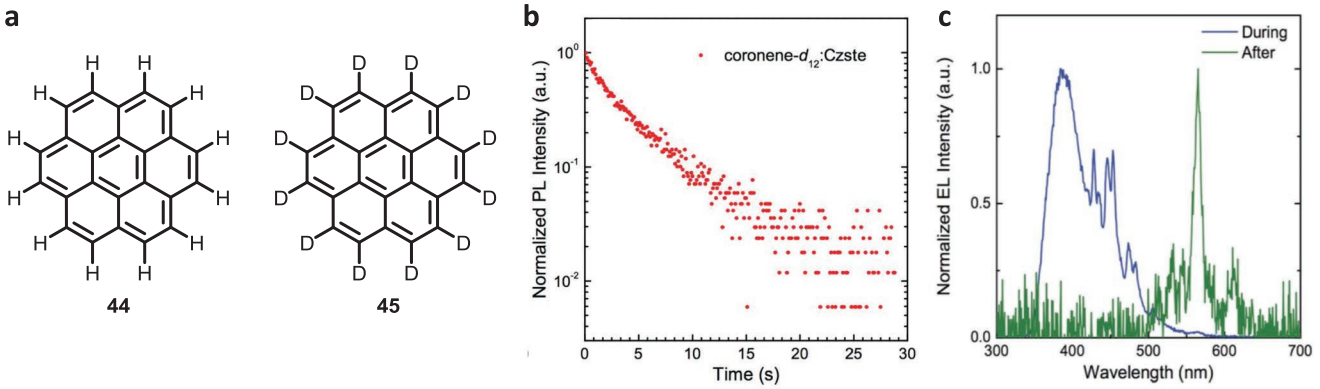

Figure 13. a) Chemical structures of coronene (**44**) and coronene-d_{12} (**45**). b) Transient PL intensity of **45**@CzSte at 560 nm. c) Electroluminescence spectra of **45**@CzSte during and after electrical excitation (blue and green lines, respectively). Reproduced with permission.[120] Copyright 2016, Wiley-VCH.

reported deep blue long-lived RTPs from triazatruxenes **51** and **52** (Figure 14a). The average τ_p values of 2.26 s and 72.05 ms and ϕ_p values of 17.5% and 36.8% were observed when 1 wt.% **51** and **52**, respectively, were embedded in the PVA matrix. The smaller average phosphorescence lifetime of **52** in PVA compared to that of **51** was probably due to the heavy atom effect of the iodide counter ions, leading to enhanced spin-orbit coupling and faster intersystem crossing.[129] Notably, a combination of CS **48** and triazatruxene **51** in the PVA matrix at the appropriate ratio (10 wt.% **48** with respect to **51**) allowed white phosphorescence with a ϕ_p of 15.8% upon excitation at 346 nm, followed by a white afterglow that persisted over 7 s.

Whereas GQDs larger than coronene (**44**) have rarely been investigated for long-lived luminescence recently, Clar

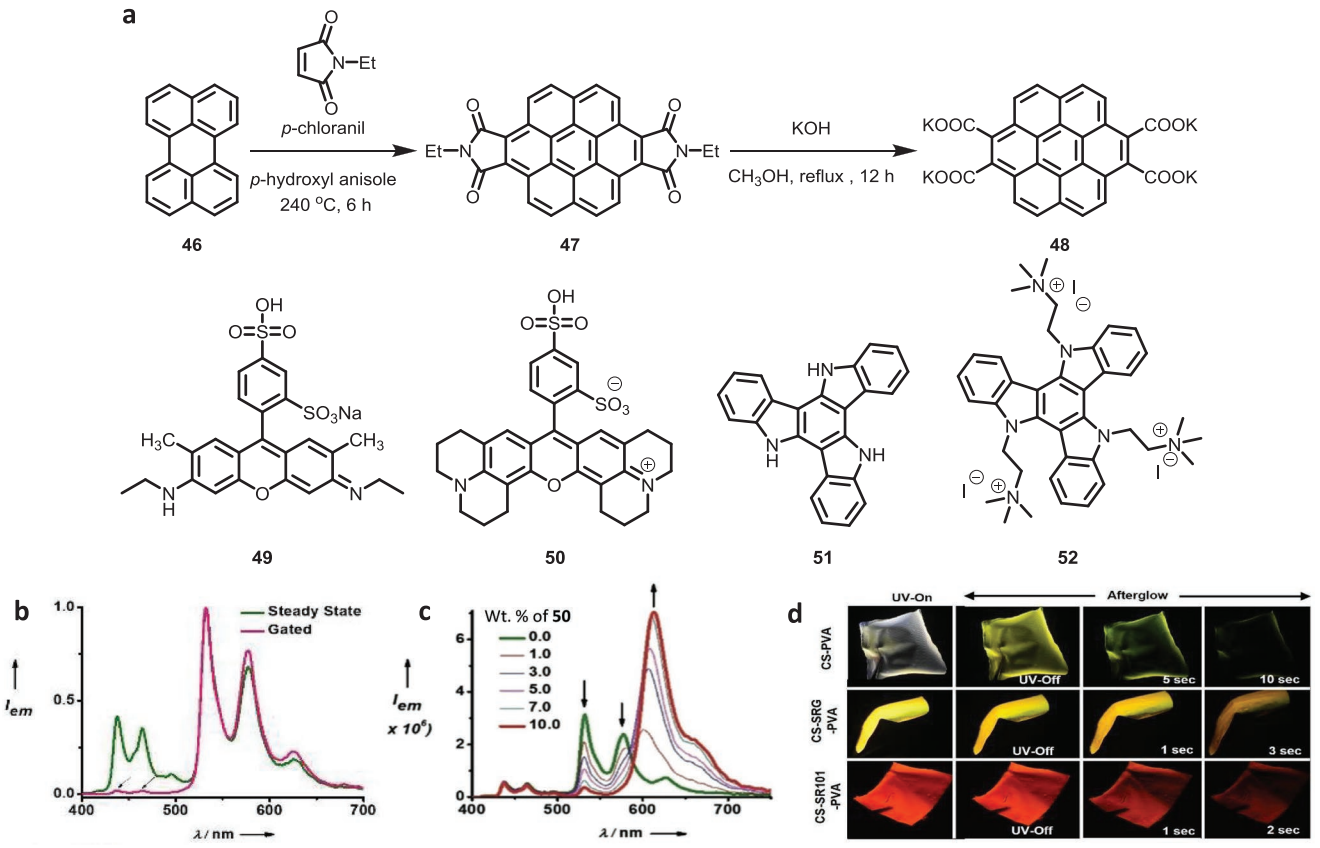

Figure 14. a) Synthesis of coronene tetracarboxylate salt (CS) **48** and chemical structures of SRG **49**, SR101 **50**, and triazatruxenes **51** and **52**. b) Steady-state and gated emission spectra of **48**-PVA film. c) Emission spectra of the CS **48**/SR101 **50**/PVA films with different ratios of **48** and **50**. d) Photographs of films of CS **48**/PVA, CS **48**/SRG **49**/PVA, and CS **48**/SR101 **50**/PVA, showing ambient afterglow properties after the cessation of UV irradiation. Reproduced with permission.[128] Copyright 2019, Wiley-VCH.

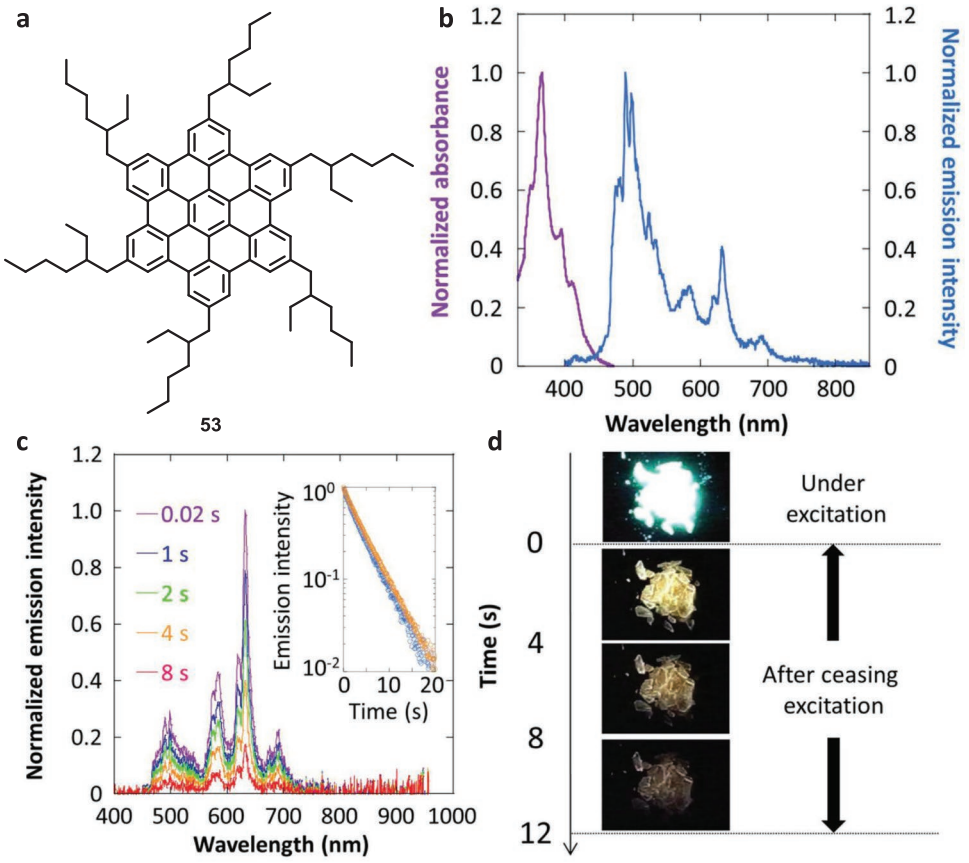

Figure 15. Chemical structure of HBC **53**. b) Solid-state absorption (purple) and emission (blue) spectra of **53** (0.3 w%) embedded in β-estradiol by excitation at 360 nm under ambient conditions. c) Emission spectrum after the cessation of excitation at 360 nm under ambient conditions at RT, showing the intensity changes. Inset: decay characteristics of the emission at 628 nm (orange) and 490 nm (blue). d) Photographs showing the changes in luminescence from **53** (0.3 w%) embedded in β-estradiol under excitation and after the cessation of excitation under ambient conditions. Reproduced with permission.[130] Copyright 2017, Wiley-VCH.

and Ironside noted long-life orange-yellow phosphorescence of HBC at low temperature in their report in 1958.[131] After almost 60 years, Hirata and Vacha demonstrated that hexa(2-ethylhexyl)-HBC **53**, when embedded in β-estradiol as the host material, displays blue-green thermally activated delayed fluorescence (TADF) simultaneously with red phosphorescence under ambient conditions, leading to white afterglow (**Figure 15**).[130] The PL spectrum of **53**@β-estradiol showed well-resolved vibronic peaks (Figure 15b), similar to the spectra of similar HBC derivatives in solution, with a PL quantum yield of 9.3%, indicating that the molecules of **53** were effectively isolated in β-estradiol. After cessation of the excitation light, white afterglow emission was observed at RT with a quantum yield of 2.6% and a lifetime of 3.9 s (Figure 15c,d).[130] A relatively small energy difference of 0.48 eV between the lowest singlet excited state and the lowest triplet excited state (ΔE_{ST}) was determined for **53** based on the 0-0 transition peaks of its delayed fluorescence (469 nm) and phosphorescence (572 nm), which accounted for the occurrence of TADF. The reduction in ΔE_{ST} was ascribed to the effective separation between the two molecular orbitals associated with fluorescence, resulting from delocalization over a 2D extended aromatic core.

4. Conclusions and Outlook

In this progress report, we have summarized the recent developments in the synthesis of large PAHs as atomically precise GQDs and relevant spectroscopic studies, with a focus on their current and/or possible applications in photonics. In particular, we have highlighted the chemical synthesis of GQDs with zigzag edges, which have revealed unique optical properties, such as strong absorption/PL in the visible/NIR region, high fluorescence quantum yields, and optical gain. Multiple examples of stable and solution-processable GQDs with zigzag edges have been achieved in recent years, demonstrating fine tailoring of their size and peripheral structures and thus of their spectral features. State-of-the-art optical spectroscopic studies have permitted access to the rich photophysics of such GQDs, leading to insights into the mechanism underpinning their intriguing optical features. For instance, ultrafast spectroscopy has highlighted the role of zigzag edges in the optical gain properties of GQDs, possibly owing to the presence of localized and emissive edge states. On the other hand, the interplay between the gain band and absorption from dark and likely charged states plays an important role in determining both the spectral shape/position of ASE and the pumping threshold necessary to achieve lasing action.

These unique properties have prompted the exploitation of GQDs in a range of applications, where high and tunable emission and photostability are highly desirable. These applications range from fundamental demonstration of exciton–photon strong coupling, ultrafast resonant optical switching, and single-photon emission to more practical uses as active material in lasers covering the visible–NIR region, in photodetectors, and as stable fluorophores for superresolution imaging. Based on these promising results, the next steps could be further exploration of GQDs with novel aromatic core structures as well as their peripheral functionalization to improve and tune their properties for specific applications, for example, to achieve lower-energy emission, lower ASE thresholds, and sensitivity to external stimuli relevant to sensing applications. On the other hand, recent advancements in PAH synthesis have paved new avenues towards chiral GQDs with nonplanar, helical substructures, which display intriguing chiroptical properties. Moreover, the long-lived phosphorescence properties of PAHs have recently been revisited, demonstrating the potential of GQDs for attaining multicolor, intense afterglow emission. These results thus highlight the significance of the chemical synthesis of such atomically precise GQDs as advanced optical materials with tunable structure-dependent properties and suggest their promise in photonic applications.

Acknowledgements

G.M.P. and Goudappagouda contributed equally to this work. G.M.P. thanks Fondazione Cariplo (grant no 2018-0979) for financial support. G. and A.N. are grateful for the financial support by the Okinawa Institute of Science and Technology Graduate University and JSPS KAKENHI Grant Number JP19K24686. Q.C. and A.N. appreciate the financial support of the Max Planck Society, the ANR-DFG NLE Grant GRANAO by DFG 431450789 and the FLAG-ERA Grant OPERA by DFG 437130745. F.S. acknowledges the financial support of the European Research Council (ERC) under the European Union's Horizon 2020 research and innovation program "PAIDEIA", grant agreement 816313.

Open access funding enabled and organized by Projekt DEAL.

Conflict of Interest

The authors declare no conflict of interest.

Keywords

graphene quantum dots, light–matter interaction, nanographene, optical spectroscopy, photonics

Received: March 11, 2021
Revised: June 6, 2021
Published online:

[1] J. Clark, G. Lanzani, *Nat. Photonics* **2010**, *4*, 438.
[2] M. Annadhasan, S. Basak, N. Chandrasekhar, R. Chandrasekar, *Adv. Opt. Mater.* **2020**, *8*, 2000959.
[3] O. Ostroverkhova, *Chem. Rev.* **2016**, *116*, 13279.
[4] G. M. Paternò, *Nanoscale Characterisation and Neutron Damage Testing of Organic Semiconductors*, University College London, London **2016**.
[5] Q. Wei, N. Fei, A. Islam, T. Lei, L. Hong, R. Peng, X. Fan, L. Chen, P. Gao, Z. Ge, *Adv. Opt. Mater.* **2018**, *6*, 1800512.
[6] Y. Zou, S. Gong, G. Xie, C. Yang, *Adv. Opt. Mater.* **2018**, *6*, 1800568.
[7] J. J. M. Halls, C. A. Walsh, N. C. Greenham, E. A. Marseglia, R. H. Friend, S. C. Moratti, A. B. Holmes, *Nature* **1995**, *376*, 498.
[8] J. Hou, O. Inganas, R. H. Friend, F. Gao, *Nat. Mater.* **2018**, *17*, 119.
[9] I. Ierides, A. Zampetti, F. Cacialli, *Curr. Opin. Green Sustain. Chem.* **2019**, *17*, 15.
[10] J. H. Burroughes, D. D. C. Bradley, A. R. Brown, R. N. Marks, K. Mackay, R. H. Friend, P. L. Burns, A. B. Holmes, *Nature* **1990**, *347*, 539.
[11] S. J. Zou, Y. Shen, F. M. Xie, J. De Chen, Y. Q. Li, J. X. Tang, *Mater. Chem. Front.* **2020**, *4*, 788.
[12] A. Zampetti, A. Minotto, F. Cacialli, *Adv. Funct. Mater.* **2019**, *29*, 1807623.
[13] N. Tessler, G. J. Denton, R. H. Friend, *Nature* **1996**, *382*, 695.
[14] I. D. W. Samuel, G. A. Turnbull, *Chem. Rev.* **2007**, *107*, 1272.
[15] Y. Jiang, Y.-Y. Liu, X. Liu, H. Lin, K. Gao, W.-Y. Lai, W. Huang, *Chem. Soc. Rev.* **2020**, *49*, 5885.
[16] A. Narita, X. Y. Wang, X. Feng, K. Müllen, *Chem. Soc. Rev.* **2015**, *44*, 6616.
[17] X. Y. Wang, X. Yao, K. Müllen, *Sci. China Chem.* **2019**, *62*, 1099.
[18] W. Chen, F. Yu, Q. Xu, G. Zhou, Q. Zhang, *Adv. Sci.* **2020**, *7*, 1903766.
[19] I. Pozo, E. Guitián, D. Pérez, D. Peña, *Acc. Chem. Res.* **2019**, *52*, 2472.
[20] H. Ito, Y. Segawa, K. Murakami, K. Itami, *J. Am. Chem. Soc.* **2019**, *141*, 3.
[21] I. R. Márquez, S. Castro-Fernández, A. Millán, A. G. Campaña, *Chem. Commun.* **2018**, *54*, 6705.
[22] L. Cao, M. J. Meziani, S. Sahu, Y. P. Sun, *Acc. Chem. Res.* **2013**, *46*, 171.
[23] R. Liu, D. Wu, X. Feng, K. Müllen, *J. Am. Chem. Soc.* **2011**, *133*, 15221.
[24] S. Zhu, L. Wang, B. Li, Y. Song, X. Zhao, G. Zhang, S. Zhang, S. Lu, J. Zhang, H. Wang, H. Sun, B. Yang, *Carbon* **2014**, *77*, 462.
[25] X. Yan, B. Li, L. S. Li, *Acc. Chem. Res.* **2013**, *46*, 2254.
[26] X.-Y. Wang, A. Narita, K. Müllen, *Nat. Rev. Chem.* **2018**, *2*, 0100.
[27] X. Xu, K. Müllen, A. Narita, *Bull. Chem. Soc. Jpn.* **2020**, *93*, 490.
[28] G. Lanzani, in *The Photophysics behind Photovoltaics and Photonics*, Wiley-VCH Verlag GmbH & Co. KGaA, Weinheim, Germany, **2012**, pp. 53–69.
[29] Y. W. Son, M. L. Cohen, S. G. Louie, *Nature* **2006**, *444*, 347.
[30] B. Trauzettel, D. V. Bulaev, D. Loss, G. Burkard, *Nat. Phys.* **2007**, *3*, 192.
[31] S. Mishra, D. Beyer, R. Berger, J. Liu, O. Gröning, J. I. Urgel, K. Müllen, P. Ruffieux, X. Feng, R. Fasel, *J. Am. Chem. Soc.* **2020**, *142*, 1147.
[32] R. Rieger, K. Müllen, *J. Phys. Org. Chem.* **2010**, *23*, 315.
[33] M. R. Younis, G. He, J. Lin, P. Huang, *Front. Chem.* **2020**, *8*, 424.
[34] A. Xu, G. Wang, Y. Li, H. Dong, S. Yang, P. He, G. Ding, *Small* **2020**, *16*, 2004621.
[35] K. Nekoueian, M. Amiri, M. Sillanpää, F. Marken, R. Boukherroub, S. Szunerits, *Chem. Soc. Rev.* **2019**, *48*, 4281.
[36] S. Yang, W. Li, C. Ye, G. Wang, H. Tian, C. Zhu, P. He, G. Ding, X. Xie, Y. Liu, Y. Lifshitz, S. T. Lee, Z. Kang, M. Jiang, *Adv. Mater.* **2017**, *29*, 1605625.
[37] M. H. M. Facure, R. Schneider, L. A. Mercante, D. S. Correa, *Environ. Sci.: Nano* **2020**, *7*, 3710.
[38] Y. Du, S. Guo, *Nanoscale* **2016**, *8*, 2532.

[39] A. Cadranel, J. T. Margraf, V. Strauss, T. Clark, D. M. Guldi, *Acc. Chem. Res.* **2019**, *52*, 955.
[40] H. Sun, L. Wu, W. Wei, X. Qu, *Mater. Today* **2013**, *16*, 433.
[41] S. Y. Lim, W. Shen, Z. Gao, *Chem. Soc. Rev.* **2015**, *44*, 362.
[42] M. Grzybowski, B. Sadowski, H. Butenschön, D. T. Gryko, *Angew. Chem., Int. Ed.* **2020**, *59*, 2998.
[43] J. R. Dias, *J. Phys. Org. Chem.* **2002**, *15*, 94.
[44] S. E. Stein, R. L. Brown, *J. Am. Chem. Soc.* **1987**, *109*, 3721.
[45] L. Zhi, K. Müllen, *J. Mater. Chem.* **2008**, *18*, 1472.
[46] J. Liu, X. Feng, *Angew. Chem., Int. Ed.* **2020**, *59*, 23386.
[47] Z. Sun, Q. Ye, C. Chi, J. Wu, *Chem. Soc. Rev.* **2012**, *41*, 7857.
[48] Z. Zeng, X. Shi, C. Chi, J. T. López Navarrete, J. Casado, J. Wu, *Chem. Soc. Rev.* **2015**, *44*, 6578.
[49] X. Xu, Q. Chen, A. Narita, Y. Gosei, *J. Synth. Org. Chem., Jpn.* **2020**, *78*, 1094.
[50] W. Zeng, J. Wu, *Chem* **2021**, *7*, 358.
[51] A. Konishi, Y. Hirao, K. Matsumoto, H. Kurata, R. Kishi, Y. Shigeta, M. Nakano, K. Tokunaga, K. Kamada, T. Kubo, *J. Am. Chem. Soc.* **2013**, *135*, 1430.
[52] A. Konishi, Y. Hirao, M. Nakano, A. Shimizu, E. Botek, B. Champagne, D. Shiomi, K. Sato, T. Takui, K. Matsumoto, H. Kurata, T. Kubo, *J. Am. Chem. Soc.* **2010**, *132*, 11021.
[53] M. R. Ajayakumar, Y. Fu, J. Ma, F. Hennersdorf, H. Komber, J. J. Weigand, A. Alfonsov, A. A. Popov, R. Berger, J. Liu, K. Müllen, X. Feng, *J. Am. Chem. Soc.* **2018**, *140*, 6240.
[54] Y. Ni, T. Y. Gopalakrishna, H. Phan, T. S. Herng, S. Wu, Y. Han, J. Ding, J. Wu, *Angew. Chem., Int. Ed.* **2018**, *57*, 9697.
[55] J. J. Shen, Y. Han, S. Dong, H. Phan, T. S. Herng, T. Xu, J. Ding, C. Chi, *Angew. Chem., Int. Ed.* **2021**, *60*, 4464.
[56] M. Ball, Y. Zhong, Y. Wu, C. Schenck, F. Ng, M. Steigerwald, S. Xiao, C. Nuckolls, *Acc. Chem. Res.* **2015**, *48*, 267.
[57] R. D. Broene, F. Diederich, *Tetrahedron Lett.* **1991**, *32*, 5227.
[58] Y. C. Chen, T. Cao, C. Chen, Z. Pedramrazi, D. Haberer, D. G. De Oteyza, F. R. Fischer, S. G. Louie, M. F. Crommie, *Nat. Nanotechnol.* **2015**, *10*, 156.
[59] S. Osella, A. Narita, M. G. Schwab, Y. Hernandez, X. Feng, K. Müllen, D. Beljonne, *ACS Nano* **2012**, *6*, 5539.
[60] X. Yan, X. Cui, B. Li, L. S. Li, *Nano Lett.* **2010**, *10*, 1869.
[61] J. Wu, W. Pisula, K. Müllen, *Chem. Rev.* **2007**, *107*, 718.
[62] V. Bonal, R. Muñoz-Mármol, F. Gordillo Gámez, M. Morales-Vidal, J. M. Villalvilla, P. G. Boj, J. A. Quintana, Y. Gu, J. Wu, J. Casado, M. A. Díaz-García, *Nat. Commun.* **2019**, *10*, 3327.
[63] F. Lombardi, A. Lodi, J. Ma, J. Liu, M. Slota, A. Narita, W. K. Myers, K. Müllen, X. Feng, L. Bogani, *Science* **2019**, *366*, 1107.
[64] J. Liu, P. Ravat, M. Wagner, M. Baumgarten, X. Feng, K. Müllen, *Angew. Chem., Int. Ed.* **2015**, *54*, 12442.
[65] Y. Gu, Y. G. Tullimilli, J. Feng, H. Phan, W. Zeng, J. Wu, *Chem. Commun.* **2019**, *55*, 5567.
[66] Y. Gu, X. Wu, T. Y. Gopalakrishna, H. Phan, J. Wu, *Angew. Chem., Int. Ed.* **2018**, *57*, 6541.
[67] T. Dumslaff, B. Yang, A. Maghsoumi, G. Velpula, K. S. Mali, C. Castiglioni, S. De Feyter, M. Tommasini, A. Narita, X. Feng, K. Müllen, *J. Am. Chem. Soc.* **2016**, *138*, 4726.
[68] T. Dumslaff, Y. Gu, G. M. Paternò, Z. Qiu, A. Maghsoumi, M. Tommasini, X. Feng, F. Scotognella, A. Narita, K. Müllen, *Chem. Sci.* **2020**, *11*, 12816.
[69] Z. Wang, Ž. Tomović, M. Kastler, R. Pretsch, F. Negri, V. Enkelmann, K. Müllen, *J. Am. Chem. Soc.* **2004**, *126*, 7794.
[70] X. Feng, W. Pisula, K. Müllen, *J. Am. Chem. Soc.* **2007**, *129*, 14116.
[71] M. Kastler, J. Schmidt, W. Pisula, D. Sebastiani, K. Müllen, *J. Am. Chem. Soc.* **2006**, *128*, 9526.
[72] G. M. Paternò, Q. Chen, X. Y. Wang, J. Liu, S. G. Motti, A. Petrozza, X. Feng, G. Lanzani, K. Müllen, A. Narita, F. Scotognella, *Angew. Chem., Int. Ed.* **2017**, *56*, 6753.
[73] Q. Chen, S. Thoms, S. Stöttinger, D. Schollmeyer, K. Müllen, A. Narita, T. Basché, *J. Am. Chem. Soc.* **2019**, *141*, 16439.
[74] G. M. Paternò, L. Nicoli, Q. Chen, K. Müllen, A. Narita, G. Lanzani, F. Scotognella, *J. Phys. Chem. C* **2018**, *122*, 25007.
[75] G. M. Paternò, L. Moretti, A. J. Barker, Q. Chen, K. Müllen, A. Narita, G. Cerullo, F. Scotognella, G. Lanzani, *Adv. Funct. Mater.* **2019**, *29*, 1805249.
[76] D. M. Coles, Q. Chen, L. C. Flatten, J. M. Smith, K. Müllen, A. Narita, D. G. Lidzey, *Nano Lett.* **2017**, *17*, 5521.
[77] X. Liu, S. Y. Chen, Q. Chen, X. Yao, M. Gelléri, S. Ritz, S. Kumar, C. Cremer, K. Landfester, K. Müllen, S. H. Parekh, A. Narita, M. Bonn, *Angew. Chem., Int. Ed.* **2020**, *59*, 496.
[78] P. Fantuzzi, A. Candini, Q. Chen, X. Yao, T. Dumslaff, N. Mishra, C. Coletti, K. Müllen, A. Narita, M. Affronte, *J. Phys. Chem. C* **2019**, *123*, 26490.
[79] Q. Chen, D. Wang, M. Baumgarten, D. Schollmeyer, K. Müllen, A. Narita, *Chem. - Asian J.* **2019**, *14*, 1703.
[80] Q. Chen, D. Schollmeyer, K. Müllen, A. Narita, *J. Am. Chem. Soc.* **2019**, *141*, 19994.
[81] R. Muñoz-Mármol, V. Bonal, G. M. Paternò, A. M. Ross, P. G. Boj, J. M. Villalvilla, J. A. Quintana, F. Scotognella, C. D'Andrea, S. Sardar, G. Lanzani, Y. Gu, J. Wu, M. A. Díaz-García, *Nanomaterials* **2020**, *10*, 1525.
[82] Y. Zou, V. Bonal, S. Moles Quintero, P. G. Boj, J. M. Villalvilla, J. A. Quintana, G. Li, S. Wu, Q. Jiang, Y. Ni, J. Casado, M. A. Díaz-García, J. Wu, *Angew. Chem., Int. Ed.* **2020**, *59*, 14927.
[83] W. Zeng, Q. Qi, J. Wu, *Sci. Bull.* **2015**, *60*, 1266.
[84] X. Yao, X.-Y. Wang, C. Simpson, G. M. Paternò, M. Guizzardi, M. Wagner, G. Cerullo, F. Scotognella, M. D. Watson, A. Narita, K. Müllen, *J. Am. Chem. Soc.* **2019**, *141*, 4230.
[85] Y. Yang, R. C. Da Costa, M. J. Fuchter, A. J. Campbell, *Nat. Photonics* **2013**, *7*, 634.
[86] G. Gingras, *Chem. Soc. Rev.* **2013**, *42*, 1051.
[87] Y. Nakakuki, T. Hirose, H. Sotome, H. Miyasaka, K. Matsuda, *J. Am. Chem. Soc.* **2018**, *140*, 4317.
[88] C. Li, Y. Yang, Q. Miao, *Chem. - Asian J.* **2018**, *13*, 884.
[89] C. M. Cruz, S. Castro-Fernández, E. Maçôas, J. M. Cuerva, A. G. Campaña, *Angew. Chem., Int. Ed.* **2018**, *57*, 14782.
[90] D. Reger, P. Haines, F. W. Heinemann, D. M. Guldi, N. Jux, *Angew. Chem., Int. Ed.* **2018**, *57*, 5938.
[91] Y. Zhu, Z. Xia, Z. Cai, Z. Yuan, N. Jiang, T. Li, Y. Wang, X. Guo, Z. Li, S. Ma, D. Zhong, Y. Li, J. Wang, *J. Am. Chem. Soc.* **2018**, *140*, 4222.
[92] P. J. Evans, J. Ouyang, L. Favereau, J. Crassous, I. Fernández, J. Perles, N. Martín, *Angew. Chem., Int. Ed.* **2018**, *57*, 6774.
[93] M. M. Martin, F. Hampel, N. Jux, *Chem. - Eur. J.* **2020**, *26*, 10210.
[94] C. Dusold, D. I. Sharapa, F. Hampel, A. Hirsch, *Chem. - Eur. J.* **2021**, *27*, 2332.
[95] M. A. Medel, R. Tapia, V. Blanco, D. Miguel, S. P. Morcillo, A. G. Campaña, *Angew. Chem., Int. Ed.* **2021**, *60*, 6094.
[96] S. Castro-Fernández, C. M. Cruz, I. F. A. Mariz, I. R. Márquez, V. G. Jiménez, L. Palomino-Ruiz, J. M. Cuerva, E. Maçôas, A. G. Campaña, *Angew. Chem., Int. Ed.* **2020**, *59*, 7139.
[97] Y. Wang, Z. Yin, Y. Zhu, J. Gu, Y. Li, J. Wang, *Angew. Chem., Int. Ed.* **2019**, *58*, 587.
[98] Y. Zhu, X. Guo, Y. Li, J. Wang, *J. Am. Chem. Soc.* **2019**, *141*, 5511.
[99] Y. Hu, X. Y. Wang, P. X. Peng, X. C. Wang, X. Y. Cao, X. Feng, K. Müllen, A. Narita, *Angew. Chem., Int. Ed.* **2017**, *56*, 3374.
[100] Y. Hu, G. M. Paternò, X. Y. Wang, X. C. Wang, M. Guizzardi, Q. Chen, D. Schollmeyer, X. Y. Cao, G. Cerullo, F. Scotognella, K. Müllen, A. Narita, *J. Am. Chem. Soc.* **2019**, *141*, 12797.
[101] S. Hirata, *Adv. Opt. Mater.* **2017**, *5*, 1700116.
[102] S. Xu, R. Chen, C. Zheng, W. Huang, *Adv. Mater.* **2016**, *28*, 9920.

[103] M. Kasha, *Chem. Rev.* **1947**, *41*, 401.
[104] N. J. Turro, M. Aikawa, *J. Am. Chem. Soc.* **1980**, *102*, 4866.
[105] N. Gan, H. Shi, Z. An, W. Huang, *Adv. Funct. Mater.* **2018**, *28*, 1802657.
[106] W. Zhao, Z. He, B. Z. Tang, *Nat. Rev. Mater.* **2020**, *5*, 869.
[107] X. Ma, J. Wang, H. Tian, *Acc. Chem. Res.* **2019**, *52*, 738.
[108] F. B. Dias, K. N. Bourdakos, V. Jankus, K. C. Moss, K. T. Kamtekar, V. Bhalla, J. Santos, M. R. Bryce, A. P. Monkman, *Adv. Mater.* **2013**, *25*, 3707.
[109] A. Forni, E. Lucenti, C. Botta, E. Cariati, *J. Mater. Chem. C* **2018**, *6*, 4603.
[110] X. Yang, G. Zhou, W. Y. Wong, *Chem. Soc. Rev.* **2015**, *44*, 8484.
[111] Q. Li, Y. Tang, W. Hu, Z. Li, *Small* **2018**, *14*, 1801560.
[112] M. Baroncini, G. Bergamini, P. Ceroni, *Chem. Commun.* **2017**, *53*, 2081.
[113] A. D. Nidhankar, Goudappagouda, V. C. Wackchaure, S. S. Babu, *Chem. Sci.* **2021**, *12*, 4216.
[114] S. S. Babu, J. Aimi, H. Ozawa, N. Shirahata, A. Saeki, S. Seki, A. Ajayaghosh, H. Möhwald, T. Nakanishi, *Chem. - Eur. J.* **2012**, *51*, 3391.
[115] S. S. Babu, M. J. Hollamby, J. Aimi, H. Ozawa, A. Saeki, S. Seki, K. Kobayashi, K. Hagiwara, M. Yoshizawa, H. Möhwald, T. Nakanishi, *Nat. Commun.* **2013**, *4*, 1969.
[116] Goudappagouda, A. Manthanath, V. C. Wakchaure, K. C. Ranjeesh, T. Das, K. Vanka, T. Nakanishi, S. S. Babu, *Angew. Chem., Int. Ed* **2019**, *58*, 2284.
[117] J. L. Kropp, W. R. Dawson, *J. Phys. Chem.* **1967**, *71*, 4499.
[118] J. Weijun, L. Changsong, *Anal. Chem.* **1993**, *65*, 863.
[119] I. Goryacheva, S. Shtykov, G. Melnikov, E. Fedorenko, *Environ. Chem. Lett.* **2003**, *1*, 82.
[120] R. Kabe, N. Notsuka, K. Yoshida, C. Adachi, *Adv. Mater.* **2016**, *28*, 655.
[121] H. Mieno, R. Kabe, N. Notsuka, M. D. Allendorf, C. Adachi, *Adv. Opt. Mater.* **2016**, *4*, 1015.
[122] S. Hirata, M. Vacha, *J. Phys. Chem. Lett.* **2017**, *8*, 3683.
[123] S. Hirata, K. Totani, T. Yamashita, C. Adachi, M. Vacha, *Nat. Mater.* **2014**, *13*, 938.
[124] R. Banerjee, A. Phan, B. Wang, C. Knobler, H. Furukawa, M. O'Keeffe, O. M. Yaghi, *Science* **2008**, *319*, 939.
[125] Q. Wang, D. Astruc, *Chem. Rev.* **2020**, *120*, 1438.
[126] Y. X. Tan, F. Wang, J. Zhang, *Chem. Soc. Rev.* **2018**, *47*, 2130.
[127] T. Ohsaka, F. Izumi, Y. Fujiki, *J. Raman Spectrosc.* **1978**, *7*, 321.
[128] S. Kuila, S. J. George, *Angew. Chem., Int. Ed* **2020**, *59*, 9393.
[129] S. Kuila, S. Garain, S. Bandi, S. J. George, *Adv. Funct. Mater.* **2020**, *30*, 2003693.
[130] S. Hirata, M. Vacha, *Adv. Opt. Mater.* **2017**, *5*, 1600996.
[131] C. T. Clar, E. Ironside, *Proc. Chem. Soc.* **1958**, 150.

Giuseppe M. Paternò is a postdoctoral researcher at the Center for Nanoscience and Technology (CNST) of the Italian Institute of Technology. He obtained a Ph.D. degree in physics at the University College London in 2017. His current research topics include photonics and spectroscopy of functional molecular and nanomaterials for energy and life science applications.

Goudappagouda obtained his Master's degree in chemistry from Kuvempu University, Karnataka, and his Ph.D. in chemical science under the guidance of Dr. Santhosh Babu Sukumaran at CSIR-National Chemical Laboratory (CSIR-NCL), Pune, India in 2020. He then joined Prof. Akimitsu Narita's group at the Okinawa Institute of Science and Technology Graduate University (OIST) as a postdoctoral scholar, and his current research work is focused on the synthesis of functional graphene molecules for optoelectronic and photonic applications.

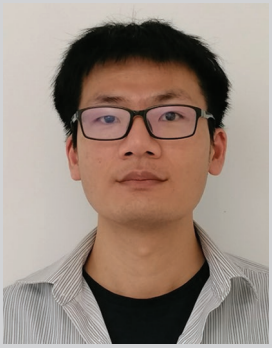

Qiang Chen is a postdoctoral researcher at the University of Oxford. He obtained his Ph.D. degree at Max Planck Institute for Polymer Research in 2019 under the supervision of Prof. Dr. Klaus Müllen and Prof. Dr. Akimitsu Narita, where he worked on the synthesis of nanographenes with unique optoelectronic properties. His current research topics include the synthesis of novel π-conjugated molecules and their applications in molecular electronic devices.

Guglielmo Lanzani is the director of the Center for Nanoscience and Technology (CNST) of the Italian Institute of Technology and full professor in physics at the Politecnico di Milano. His research activity includes the science and technology of nanostructured and molecular materials (organic semiconductors, carbon nanotubes, and semiconductor nanocrystals) for application in energy, neuroscience, and medicine.

Francesco Scotognella is associate professor in physics at Politecnico di Milano, since 2018. He obtained a Ph.D. degree in materials science in 2009 at Università di Milano-Bicocca. His research focuses on the photophysics of nanomaterials and organic molecules and optical properties of photonic structures.

Akimitsu Narita is an assistant professor at the Okinawa Institute of Science and Technology Graduate University and a part-time group leader at the Max Planck Institute for Polymer Research (MPIP). He studied chemistry at the University of Tokyo, and obtained his doctorate in chemistry at MPIP in 2014 under the supervision of Prof. Dr. Klaus Müllen. His current research focuses on the synthesis, characterizations, and applications of large polycyclic aromatic hydrocarbons as atomically precise graphene quantum dots.